Annual Report

Authors

Alfred Strasser
Sleepy Hollow, NY, USA

Friedrich Garzarolli
Fürth, Germany

Ron Adamson
Fremont, CA, USA

Kit Coleman
Ontario, Canada

Peter Rudling
ANT International, Mölnlycke, Sweden

A.N.T. INTERNATIONAL®

Advanced Nuclear Technology International
Analysvägen 5, SE-435 33 Mölnlycke
Sweden

info@antinternational.com
www.antinternational.com


Ecolabelled printed matter, 3041 0129

Disclaimer

The information presented in this report has been compiled and analysed by Advanced Nuclear Technology International Europe AB (ANT International®) and its subcontractors. ANT International has exercised due diligence in this work, but does not warrant the accuracy or completeness of the information. ANT International does not assume any responsibility for any consequences as a result of the use of the information for any party, except a warranty for reasonable technical skill, which is limited to the amount paid for this assignment by each ZIRAT/IZNA programme member.

Contents

1 Introduction (Peter Rudling)

The objective of the Annual Review of ZIRconium Alloy Technology (ZIRAT) and Information on Zirconium Alloys (IZNA) is to review and evaluate the latest developments in ZIRAT as they apply to nuclear fuel design and performance.

The objective is met through a review and evaluation of the most recent data on zirconium alloys and to identify the most important new information and discuss its significance in relation to fuel performance now and in the future. Included in the review are topics on materials research and development, fabrication, component design, and in-reactor performance presented in conferences, journals and reports.

The primary issues addressed in the review and this report is zirconium alloy research and development, fabrication, component design, ex- and in-reactor performance including:

- Regulatory bodies and utility perspectives related to fuel performance issues, fuel vendor developments of new fuel design to meet the fuel performance issues.
- Fabrication and Quality Control (QC) of zirconium manufacturing, zirconium alloy systems.
- Mechanical properties and their test methods (that are not covered in any other section in the report).
- Dimensional stability (growth and creep).
- Primary coolant chemistry and its effect on zirconium alloy component performance.
- Corrosion and hydriding mechanisms and performance of commercial alloys.
- Cladding primary failures.
- Post-failure degradation of failed fuel.
- Cladding performance in postulated accidents (Loss of Coolant Accident (LOCA), Reactivity Initiated Accident (RIA)).
- Dry storage.
- Potential Burn-up (BU) limitations.
- Current uncertainties and issues needing solution are identified throughout the report.

Background data from prior periods have been included wherever needed. The data published in this Report is only from non-proprietary sources; however, their compilation, evaluations, and conclusions in the report are proprietary to ANT International and ZIRAT/IZNA members as noted on the title page.

The authors of the report are Mr. Friedrich Garzarolli, Mr. Alfred Strasser, Dr. Ronald Adamson, Dr. Christopher Coleman and Mr. Peter Rudling, President of ANT International.

The work reported herein will be presented in two Seminars: in Clearwater Beach, FL., USA (February 1-3, 2016) and in Palma de Mallorca, Spain (March 7-9, 2016).

The Term of ZIRAT20/IZNA15 started on February 1, 2015 and ends on March 31, 2016.

All literature that we refer to in this Report is available in the ANT International Literature Database (LDB). Please contact Ms. Angela Olpretean at angela.olpretean@antinternational.com for more information.

2 Burnup achievements and key fuel performance issues (Al Strasser)

2.1 Introduction

The objective of this Section is to summarize the key performance issues that could affect fuel design, fabrication or operation of the nuclear fuel in the near term or the longer term. Topics covered include the fuel itself and the fuel assembly components made of nickel base alloys and stainless steels. The latest zirconium alloy technology is covered in subsequent Section 3 and on instead of this Section. The information sources reviewed, screened and evaluated include nearly all the related publications and technical meeting presentations of the past, approximately 18 months and focuses primarily on extended burnup data. The Section is intended to be a guide to significant, current issues related to these topics and provide an alert to items that could affect fuel related operations. The extensive volume of information involved limits the presentations to the most significant features and conclusions, and the reader is urged to refer to the referenced publications for more detail.

2.2 Trends in fuel operating conditions

2.2.1 General trends

Improved fuel reliability and operating economics are the driving forces for the changes in operating conditions, while maintaining acceptable margins to operating and regulatory safety limits. These are incentives for significant advances in materials technology, software for designing and predicting fuel performance, sophisticated instrumentation, modifications in water chemistry and methods for post-irradiation examinations. Some of these advances in technology have increased the demands on fuel performance levels and put pressure on the regulatory bodies to license operations to increased burnup levels. The types of changes in LWR operating methods intended to achieve improved safety and economics have not changed in the past years and still include:

- Annual fuel cycles extended to 18 and 24 months,
- Increased discharge burnups as high as 64 GWDf/MT batch average exposures by higher enrichments, increased number of burnable absorbers in the assemblies and in PWRs higher Li and B levels in the coolant, or enriched B in the coolant,
- Plant power uprates that range from 2 to 20%,
- More aggressive fuel management methods with increased enrichment levels and peaking factors,
- Reduced activity transport by Zn injection into the coolant,
- Improved water chemistry controls and increased monitoring,
- Component life extension with hydrogen water chemistry (HWC), noble metal chemistry (NMC) and more extensively with on-line noble metal chemistry (OLNC) in BWRs.

2.2.2 Fuel cycles

Cycle Lengths

The trend for increased fuel cycle lengths has come to a near "equilibrium" in the US with PWRs operating at an average of 500 effective full power days (EFPD) per cycle and BWRs an average of 620 EFPD per cycle, up to a maximum of about 680 days for PWRs and 720 days for BWRs. Nearly all the US BWRs are trending toward 24 month cycles except in an unusual move, Exelon changed the Clinton plant to a 12 month cycle. The older, lower power density PWRs have implemented the 24 month cycles, but fuel management limitations, specifically the reload batch sizes required, have limited implementation of 24 month cycles in the high power density plants. The economics of 24 month cycles tend to become plant specific since they depend on the balance of a variety of plant specific parameters. The potential economic gains for cycle extension have decreased in the US as the downtimes for reloading and maintenance procedures have been significantly reduced, increasing the capacity factors.

Most countries outside the US have one, winter power peak annually compared to the two, winter and summer peaks in the US, and this has tended to keep them on annual cycles. Changes in load management, economics, maintenance practices and licensing procedures have tended to change this and some countries, such as France, Belgium, Switzerland and Germany have applied both annual and 18 month cycles. The Russian fuel supplier TVEL has increased the fuel cycle length from 12 to 15 months in the 440 VVERs by increasing the enrichment from 4.2% to 4.7% in Russian, Finnish, Czech, Slovak and more recently in Hungarian plants.

Capacity Factors

The capacity factors of US plants has been tracked for 3 year periods starting with 1975–1977 until most recently for 2012–2014 [Blake, 2015]. The number of plants covered since the 2009–2011 period has been reduced from 104 to 100, to account for plants that have been permanently shut down. The median capacity of the plants has been quite constant, close to 90%, ever since the period of 2000 to 2002. The mean factors for the BWRs and PWRs have been nearly identical varying less than a 1% differential (Figure 2-1*)*. The spread between the top and bottom quartile plants as a function of years is given in Figure 2-2 and shows that the top quartile has been above 92% consistently since the 1999–2001 period and the bottom quartile has improved and levelled off in the range of about 86 to 87%. It is of interest to note that the median factor of multi-unit sites is slightly higher than for single unit sites in the 2012–2014 period; however, the reference claims that with recent ownership changes it is not clear whether these changes affect the data and whether the relationship still holds. The capacity factors for utilities that own more than one reactor site show a range of about 77 to 93% [Blake, 2015].

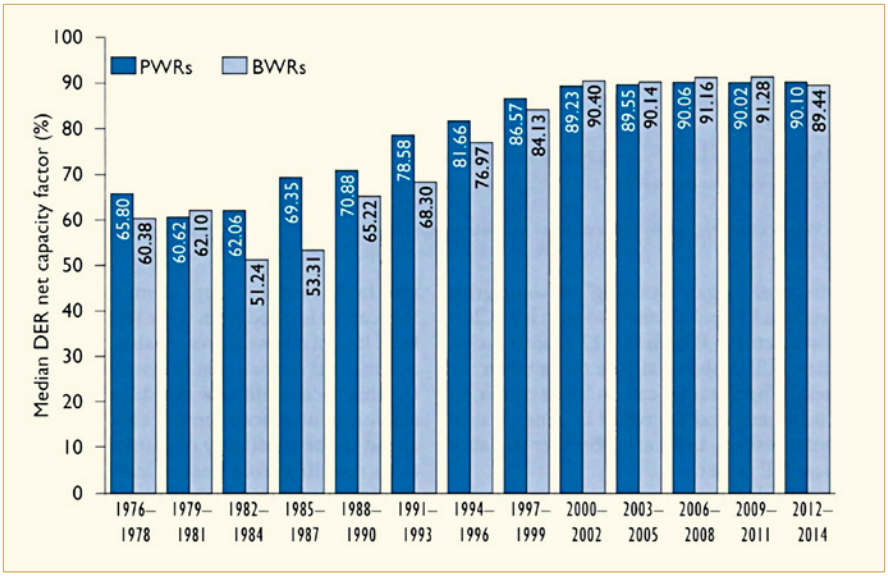

Figure 2-1: US plant capacity history. [Blake, 2015].

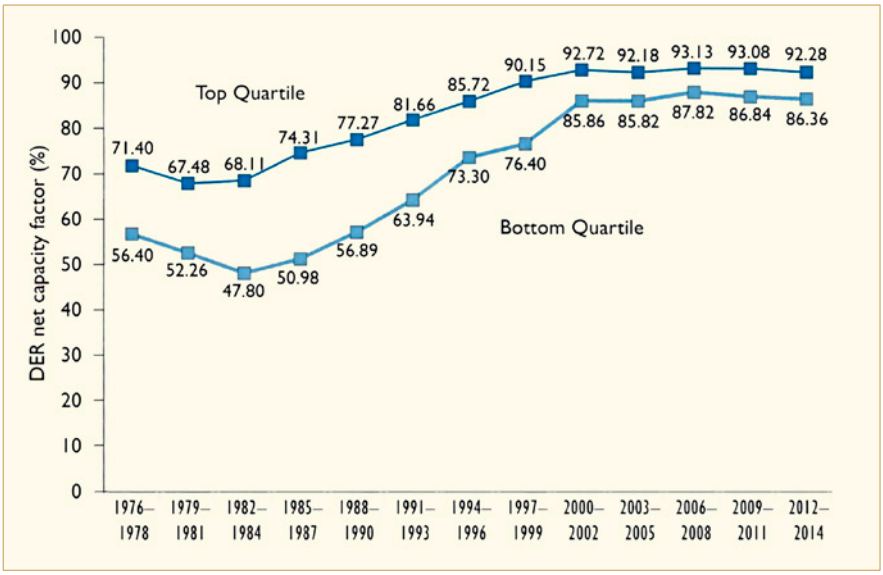

Figure 2-2: US plant top and bottom quarterly capacity factors. [Blake, 2015].

The Nuclear Energy Institute announced that the average capacity factor for all US reactors was 91.9% in 2014 – the highest ever.

Operational requirements may not require the highest capacity factor for the most economical operation; load following is a typical example. Plant performance ratings should therefore be extended beyond their capacity factors and include items such as the forced loss rate, the safety system and industrial safety performance, the scram trend, radiation exposure and other factors tracked by the Institute of Nuclear Power Operations (INPO) and World Association of Nuclear Operators (WANO). The trends through 2014 for some of these factors show general improvements over the years that exceed the goals in most cases (Figure 2-3). Radiation exposure of workers has decreased over the years to more than meet the goals for PWRs and BWRs. The fuel performance goal of 100% failure free operation has been approached with an average of 95%, but reached by failure free operation in the majority, but not all plants. Details on fuel performance are discussed in subsequent Sections.

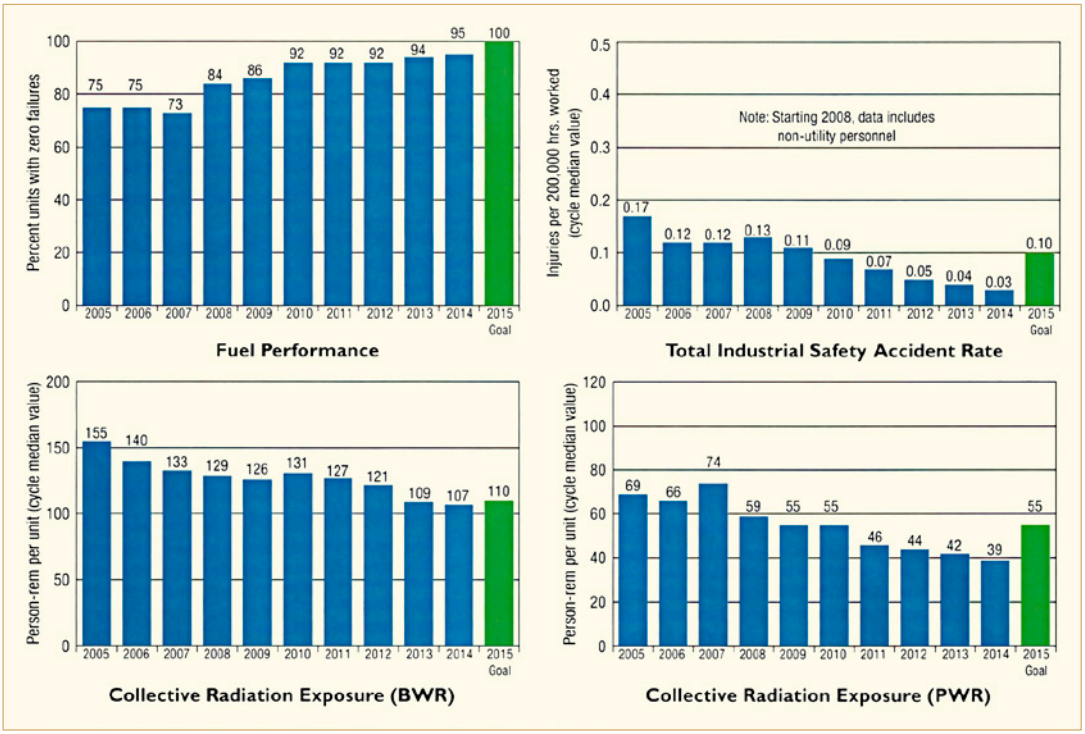

Figure 2-3: US plant performance trends. [Blake, 2015].

2.2.3 Power uprates

The power of the majority of the US operating plants has been uprated, by a maximum of 20%. While the fuel performance limits remain the same for the uprated conditions, the number of fuel assemblies operating at higher power change and the margin to the limits might be reduced. The effect of higher flow rates on hydraulic and water chemistry effects and their interaction with the fuel must also be considered. These changes have not affected the failure rate or apparently the fuel performance; however, it does increase the statistical probability of the effects of increasing power and burnup related factors on the fuel performance.

The power uprates approved in the US since 2011 are in % MWth:

BWRs:		**PWRs:**	
Limerick 1 & 2	1.65% each	Harris	1.6%
		Braidwood 1 & 2	1.6% each
Nine Mile Point 2	15.0%	Byron 1 & 2	1.6% each
Fermi 2	1.6%	McGuire 1 & 2	1.7% each
Grand Gulf 1	13.1%	St. Lucie 1 & 2	11.9% each
Monticello	12.9%	Turkey Point 3 & 4	15.0% each
Peach Bottom 2 & 3	12.4% each	Point Beach 1 & 2	17.0% each
			ANT International, 2015

Power uprate applications under review are:

PWR:	
Oconee 1, 2, & 3	1.6% each
Catawba 1	1.7%
	ANT International, 2015

The net gain of the uprating is about 620 MWe, which does not balance the 3,534 MWe lost due to the shutdown of reactors, decreasing the overall nuclear generation in the US. Power uprating is of course practiced outside the US as well.

The effect of power uprating on power distribution among the fuel assemblies was discussed in ZIRAT12/IZNA7 [Adamson et al, 2007a] and the effect on water chemistry was discussed in the ANT International Special Topical Report "Consequences of Power Uprating" [Lundgren & Riess, 2007], in the LCC3 Seminar.

2.2.4 Burnup extension

The major incentive for extended burnups is the potentially improved fuel cycle economy. Economic analyses in past ZIRAT/IZNA reports indicated that economic incentives for extending burnups beyond the 60–70 GWD/MT batch average range will disappear and that other incentives must exist in order to justify going beyond the economically optimal level. The improved economics depend in part on the decreased amount of spent fuel assemblies to be purchased, handled and disposed of. This is balanced by the increased amount of uranium and enrichment services required. The economics of decreased assemblies could also be impacted by the much longer cooling times required for high burnup and MOX fuels in spent fuel pools prior to on-site dry storage or transport to a storage facility as noted later, impacting the spent fuel pool capacities. The economic analyses are also dependent on the utility's accounting systems and as a result are utility and even plant specific.

The burnup limits are established by the regulatory agencies in each country based primarily on the thermo-mechanical performance of the fuel under normal and accident conditions as well as unintended self-imposed limits of specific designs that are below the regulatory limits. The many factors that affect and support these limits are discussed throughout the extensive ZIRAT/IZNA reports.

In addition to the thermal-mechanical limits, the additional limit of <5% peak enrichment is observed internationally. Enrichments above this limit could increase burnup, reduce batch sizes and improve fuel cycle efficiency. The effect of such designs have been evaluated and indicate that fuel cycle designs with greater enrichments may not meet thermal limits and would add uncertainties and requirements for relicensing adding costs in addition to relicensing the equipment and mechanics of handling the fuel at the fabrication plant and reactor site. The results of some studies were given in the ZIRAT16/IZNA11 Annual Report [Adamson et al, 2011].

The average batch burnups in US PWRs are currently in the range of 43–58 GWD/MT and in US BWRs in the range of 43–52 GWD/MT. The PWR burnups have leveled off and the BWRs are still increasing slightly, approaching the NRC regulatory limit of 62.5 GWD/MT peak rod. The NRC does not have any current activities to evaluate the potential increase of this limit, so that the burnups will plateau at these levels at this time.

In Europe, the batch average burnup in Switzerland has been as high as 65 GWD/MT with concurrent assembly and rod burnups of 68 and 73 GWD/MT burnups respectively. This has been possible, in part, due to the greater margin to regulatory limits in some countries. The burnup ranges by countries are compared to their regulatory limits in Table 2-1.

Table 2-1: Maximum burn-up achieved vs. regulatory limits, (excludes LTAs).

	BU (GWD/MT)				
Country	**Batch**	**Assembly**	**Rod**	**Pellet**	**Regulatory Limit**
USA	57	58	62	73	62.5 peak rod
Belgium		50-55			55 UO_2 assy., 50 MOX assy.
Czech Republic	51	56	61		60 peak rod
Finland	45.7*	48.6	58		57 assy. (for PWR)
France	47	51 UO_2 42 MOX			52 assy.
Germany	58	62	68		65 assy.
Hungary		50	62		
Japan	50	55	62		55 UO_2 assy., 45 MOX assy.
Korean Republic	46				60 rod
Netherlands	53	56	59		60 rod
Russia	60	65			
Spain	50.4	57.4	61.7	69	
Sweden	47	57.2	64	65	60 assy., 64 rod
Switzerland	64	68	73		80 pellet
Taiwan					60 rod (P), 54 assy. (B)
UK	44.3	46.5	50		55 pellet
Ukraine		50			
*Current batch design for 50 GWD/MT in BWR					
ANT International, 2015					

The Ringhals plants in Sweden have plans to target >65 GWD/MT assembly burnups with the Westinghouse Next Generation Fuel (NGF) [Chapin et al, 2013]. Westinghouse has developed the PAD5 version of their fuel performance code based on input data from the irradiation of 8 rods to 70 GWD/MT and 30 rods to 75 GWD/MT [Long et al, 2013]. The Russians have a goal to reach 70–80 GWD/MT assembly burnup with the fuel in their advanced VVER 1200 plant [Ivanova et al, 2013].

The lead test assemblies (LTAs) used to test new design concepts and materials are licensed to higher burnups than the reload batches for power production. Fuel rod burnups of close to 100 GWD/MT have been achieved by past PWR LTAs. The most recent reports of LTAs and their currently achieved burnups are listed in Table 2-2. Their goal burnups are not available. The Table lists the advanced claddings applied, most of which have been used in reload quantities as well. The clad compositions are given in Table 2-3 and compared to the original Zircaloy-2 and -4 that were used in the original fuel designs.

Table 2-2: Exposure of most recent design LTAs.

Reactor	Vendor	LTA design	Cladding	Channel	GWD/MT	Reference
BWR	GNF	GNF2	Ziron		61	[Cantonwine et al, 2015a]
					(76 peak rod node)	
				NSF test	>100 (2.2×10^{22} n/cm^2)	
	W/Sweden	SVEA96, Optima3	LK3			
				$LowT_{In}$ ZIRLO	72	[Andersson et al, 2015a]
	AREVA	ATRIUM10	Zirc2		72	[Cole et al, 2015]
		ATRIUM11	Zirc2		25	
				Z4B	25	
Reactor	**Vendor**	**LTA design**	**Cladding**	**Structural Materials**	**GWD/MT**	**Reference**
PWR	W	Various	Optimized		>70	[Halligan et al, 2015]
			ZIRLO			
	AREVA	GAIA	M5		52	[Louf et al, 2015]
			Q12		62.7	
				Unfueled clad	95	[Chabretou & Trapp-Pritsching, 2015]
				Guide tube	57.6	
				Spacer grid	48.1	
	Mitsubishi		M-MDA		73	[Watanabe et al, 2015]
					(81.2 ramp test)	

ANT International, 2015

Table 2-3: Composition of current LTA claddings and structural components (Alloying elements in weight %, the balance is zirconium).

Alloy	Sn	Nb	Fe	Cr	Ni	O
Zircaloy 2, LK3	1.20 – 1.70	-	0.07 – 0.20	0.05 – 0.15	0.03 – 0.08	0.09 – 0.15
Ziron, Z4B	1.30	-	>0.20	>0.20		
ZIRLO	1.0	1.0	0.1			0.12
LowTin, Optimized ZIRLO	0.7	1.0	0.1			0.12
NSF	1.0	1.0	0.4			
Q12	0.5	1.0	0.1			
M-MDA	0.8	0.5	0.3	0.4		
M5	<100 ppm	1.0	0.015 – 0.06			0.09 – 0.12

ANT International, 2015

The BWR claddings are essentially all slight variations of Zircaloy-2. Zircon and Z4B for channels are similar in that they have slightly increased Fe and Cr contents above the ASTM specification for Zircaloy-2. The other two vendors have changed to two similar Sn-Nb alloys, NSF and low Sn or Optimized ZIRLO, for improved dimensional stability.

The PWR claddings continue to be modifications of ZIRLO, a Sn-Nb-Fe alloy and M5, a 1% Nb alloy. The Optimized ZIRLO has a decreased Sn content for improved corrosion resistance and hydrogen pickup. The Q12 and M-MDA alloys are modified M5 compositions by the addition of small amounts of Sn and for M-MDA addition of Fe and Cr as well, to improve mechanical properties, particularly creep resistance. All the vendors that use M5 are working on modified versions that improve the mechanical properties, creep resistance in particular, and some of these are probably in LTAs, but results not published yet.

Approximate equivalence of burnup to neutron exposures can be given as 50 GWD/MT to about 1×10^{22} n/cm^2 (>1 MeV) or 17 dpa; however, this relationship depends on several factors such as enrichment, extent of moderation and neutron energy spectrum and should be evaluated for each specific case.

2.3 High burnup UO_2 and MOX fuel performance

2.3.1 Thermal conductivity

Knowledge of the effects of the fuel characteristics and the irradiation environment on fuel thermal conductivity are vital, since their value determines the fuel temperature and affects fuel performance parameters such as fission product migration and release, fuel thermal expansion and interaction with the cladding, fuel plasticity and other temperature dependent factors during both normal operations and accident conditions.

Composition and microstructure inhomogeneities that develop in the pellet's radial direction at high burnups can vary in thermal conductivity, complicating the overall fuel thermal conductivity estimates. Investigators at the Idaho National Nuclear Laboratory (INNL) [Teague et al, 2014] have taken micrographs of MOX fuel samples FO-2A and FO-2B irradiated to 6.7% and 5.8% Fissions per Initial Metal Atom (FIMA) (64 and 57 GWD/T) respectively and higher exposure samples ACO-3A and ACO-3B to 27.3 and 23.1% FIMA (227 and 204 GWD/T) samples respectively. The radial sections were divided into the various microstructural zones as shown on Figure 2-4. Each zone was then divided into microstructure based finite element meshes by means of a software called Object Oriented Finite Element, Version 2 (OOF2) supported by the National Institute of Standards and Technology (NIST) [Langer et al, 2001]. Annealing steps are then performed on each mesh to homogenize the structure by a Monte Carlo algorithm where elements are moved at random and the changes are kept if the resulting element is more homogeneous than the previous element. The meshes were then imported into the BISON fuel performance code for thermal analysis to determine the temperatures at those locations. The 2D effective thermal conductivity of the microstructures was calculated in the radial direction as a function of temperature using the equations:

$$k_{eff} = q_t \partial T / \partial x$$

$$\frac{\partial T}{\partial x} \approx \frac{T_t - T_b}{l}$$

Figure 2-5 indicates the analytic procedure which applies a constant temperature to the bottom boundary and a test heat flux over the top boundary in the direction of the coolant side. A temperature drop of 10°K or less was selected across each microstructure.

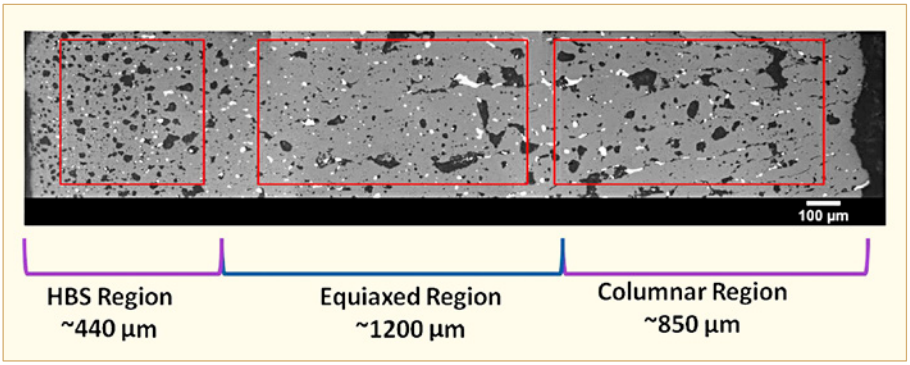

Figure 2-4: Radial cross-section of MOX sample ACO-3A with subsections used for modeling marked. [Teague et al, 2014].

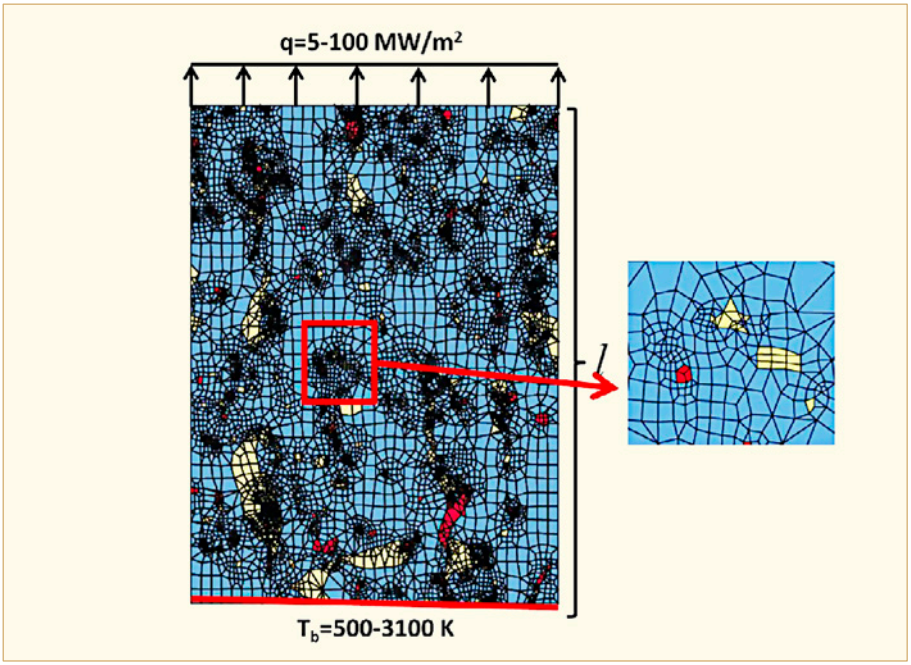

Figure 2-5: Effective thermal conductivity model, red is metallic precipitates, yellow porosity, and fuel is light blue, enlarged region of mesh is shown to right to high light varying element density to capture microstructure details [Teague et al, 2014].

The results show that in the highest burnup samples ACO-3A and -3B the equiaxed and columnar grain regions have the highest and the rim region has the lowest thermal conductivity. In the lower burnup samples the columnar region has the lowest conductivity and perhaps the rim region has not developed sufficiently to register as the lowest conductivity region (Figure 2-6 and Figure 2-7). An interesting observation made by the authors was that experimental results indicate a 55% higher thermal conductivity of the high burnup rim structure region than predicted by the analytical methods of [Walker et al, 2006]. This was postulated to be due to the healing of irradiation damage and the removal of dissolved fission products during the formation of the structure. This enhancement was not considered in this work.

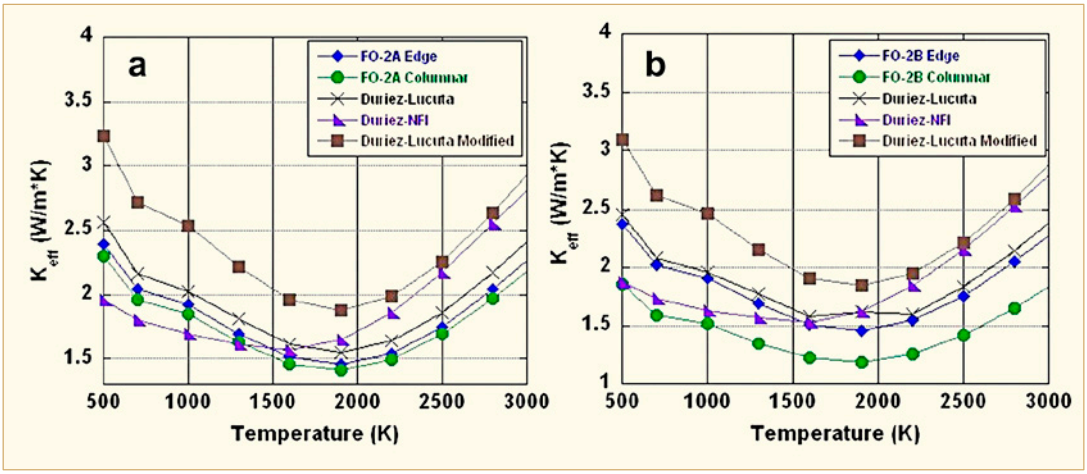

Figure 2-6: Effective thermal conductivity of MOX microstructures in samples (a) FO-2A (64 GWD/T) and (b) FO-2B (57 GWD/T) compared to analytical models [Teague et al, 2014].

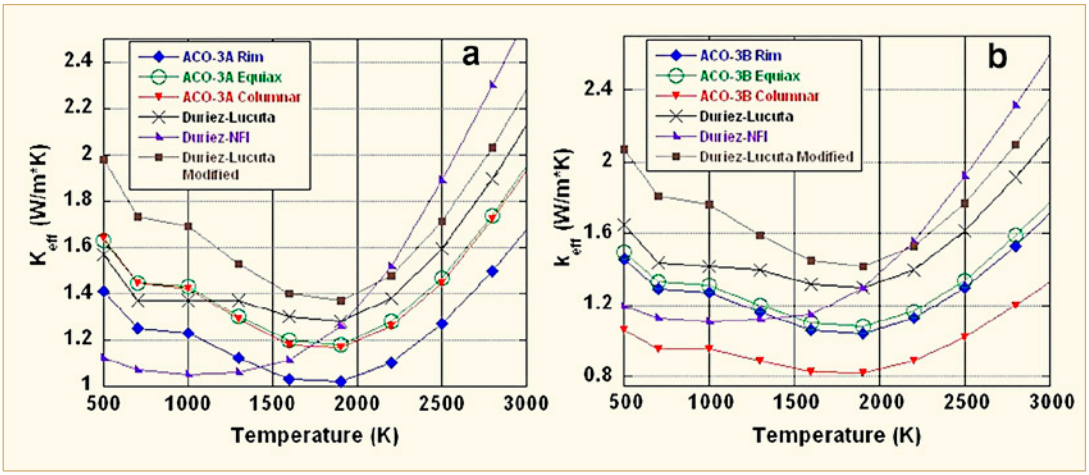

Figure 2-7: Effective thermal conductivity of MOX microstructure in (a) ACO-3A (227 GWD/T) and (b) ACO-3B (204 GWD/T) compared to analytical models [Teague et al, 2014].

The results were then compared to two other thermal conductivity models. The Durex-NFI model which is used in FRAPCON-3 is a purely empirical model for unirradiated MOX with the burnup degradation functions of UO_2 and the Duriez-Lucuta model also for unirradiated MOX which takes into account the oxygen stoichiometry and then is modified for dissolved and precipitated fission products, porosity and radiation damage. The comparisons are shown on Figure 2-6 and Figure 2-7; however the differences between the three analytical methods may not be meaningful due to the differences in modeling methods, nevertheless they show the range of responses that come from different methods.

The publication shows that the radially variable pellet thermal conductivities, due to the variable compositions and microstructures, can affect fuel temperatures and should be taken into consideration and that analytic methods to evaluate this effect have been developed.

4 Mechanical properties (Kit Coleman)

4.1 Introduction

In this section we will discuss strength and ductility. Strength is expressed in terms of properties like yield strength, burst strength and hardness. Ductility is expressed in terms such as elongation at fracture or strain-to-some limit for a particular loading condition. Fracture resistance is a combination of strength and ductility that describes the conditions to initiate and grow cracks and estimate the point of crack instability. Each of these properties is affected by their alloy composition and fabrication route, and by the consequences of their residence in a nuclear reactor in hot water. Neutron irradiation changes the microstructure thereby affecting the mechanical properties. For example, <a>-dislocation loops strengthen zirconium but when annihilated by strain, ductility and fracture toughness are reduced. Corrosion adds an oxide layer and produces hydrogen, some of which is picked-up by the components. Hydrogen is important because it forms hydrides that can lead to embrittlement. During fission, extra gasses are formed adding to the internal pressure inside a fuel rod and some elements are formed that can cause cracking in zirconium alloys, for example iodine. During service, stresses fluctuate so some allowance must be made for fatigue. Vibrations between touching surfaces can produce wear and fretting that may be so severe that protective membranes are breached. All these changes have to be accommodated to assure that components function as designed. Often each of the properties is studied separately. These individual properties are then gathered into a description of the behaviour of the whole component in models and codes. Contributions to each of these items were made during the year and examples are summarised in the following sections.

4.2 Tensile testing

In a tensile test of a material, a specimen with gauge length L, is extended ΔL at a moderate rate and the response is an increase in load, P. Specimens are usually cylinders or plates with thinned mid-sections forming the gauge length with cross-sectional area, A. Strain, ε, is estimated as elongation, $\Delta L/L$, and is dimensionless. Strength, σ, is calculated as P/A at different strains – often at 0.2% for yield strength – and has dimensions of mass/(length × time^2), which in SI has units of N/m^2 or Pascals, Pa. Standard methods are available, for example as described in ASTM International Standard Practice documents [Anonymous, 2015]; [Anonymous, 2009]. Because of the need to test samples from components, which are often highly radioactive, some tests do not meet these standards; the specimen geometry and testing conditions should always be described when reporting the test results. The results from tensile tests are used to confirm that materials conform to a technical specification for the material and to evaluate new alloys and fabrication processes and effects of in-reactor service. Tensile properties can be used to separate the effects of microstructural features on strength. The change in strength with strain is used to measure work-hardening and strain-rate sensitivity is estimated from strength with different or changes in extension rate. Along with elongation, ductility is estimated from reduction in area at fracture. Neither reduction in area nor some evaluation of work-hardening and strain-rate hardening are required by the specifications for zirconium alloys, for example, Zircaloy and Zr-2.5Nb [Anonymous, 2012]; [Anonymous, 2013a]. An effect of strain rate is implied by limiting the strain rate to the range 5×10^{-5} s^{-1} to 1.17×10^{-4} s^{-1}.

A typical well-behaved load-elongation curve is illustrated in Figure 4-1a, showing the initial linear load rise corresponding with elastic deformation followed by a decreasing curvature indicating plastic deformation and work-hardening. The yield strength is estimated by locating the stress where an offset line, mn, parallel with the elastic line, OA, intersects the stress-strain line at r. Often the offset, Om, corresponds to a plastic strain of 0.2%. ASTM Standard E8 now recognises that sometimes the test is not performed perfectly – for example, the extensometer may slip – and this deviation may contribute to the initial part of the load-elongation curve. Appendix X5 describes how to correct for these problems when estimating yield stress. One of the most common effects is illustrated in Figure 4-1b when the initial rise in load is less than the elastic response because the specimen straightens as the force is applied, due to misalignment or residual stress. Now the origin, O', is taken as the extrapolation of the elastic loading line to the strain axis and the line mn is parallel to O'A at an offset of O'm and the yield strength is at r.

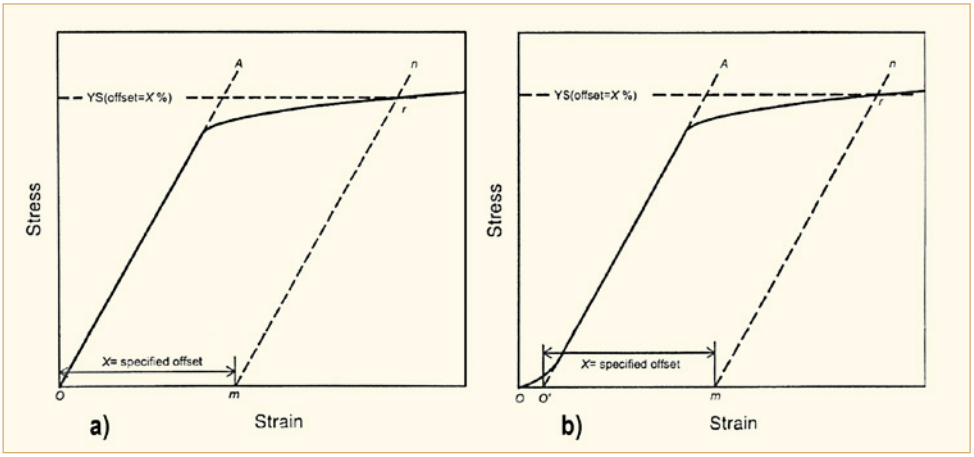

Figure 4-1: Method for estimating yield strength at r from strain offset of X%; (a) corresponds to ideal test and (b) extrapolation of the elastic line when the origin is displaced, based on [Anonymous, 2015].

Analysis of mechanical behaviour of a component, using either macroplasticity or finite element analysis, requires the uniaxial stress-strain curve to be described by equations so the multiaxial conditions may be estimated. In the elastic part of the tensile curve, stress is proportional to strain through Hooke's Law:

Eq. 4-1: $$\sigma = E.\varepsilon$$

where E = Young's elastic modulus.

Several attempts have been made to describe uniaxial tensile plastic behaviour. The relationship between true flow stress, σ_T, and true strain, ε_T, can be described by fitting work hardening to power functions, for example [Ludwig, 1909]; [Hollomon, 1945]:

Eq. 4-2: $$\sigma_T = H\,\varepsilon_T^{h}$$

where H = strength constant, h = work-hardening coefficient.

and [Ramberg & Osgood, 1943]:

Eq. 4-3: $$\varepsilon = \sigma/E\{1 + \alpha(\sigma/\sigma_0)^{m-1}\}$$

where σ_0 = yield strength and α and m are empirical constants.

Exponential functions have also been used, for example, [Voce, 1947/8]:

Eq. 4-4: $$\sigma = C\left(1-\mu.\exp(-n\varepsilon)\right)$$

where C represents the flow stress, μ represents the initial state of hardening and n represents the strain hardening.

The ability of these equations to describe the tensile tests of Zr-2.5Nb from room temperature up to 600°C has been reported [Dureja et al, 2014]. All the formulae provide good fits to the experimental data at room temperature, Figure 4-2a, and up to about 300°C but at higher temperatures, the Voce relationship deviates from experiment, Figure 4-2b. The conclusion from the study is to use Voce up to 300°C, Ramberg-Osgood between 300 and 500°C and Hollomon at higher temperatures. This description seems overly complicated, especially since the authors found the statistical fit was better than 95% over the full temperature range using either Hollomon or Ramberg-Osgood equations. A form of Eq. 4-2 is used by the US NRC in their codes for calculating stress and plastic deformation in Zircaloy fuel cladding, especially for accident analysis where the fit seems to be very good at high temperatures [Siefken et al, 2001].

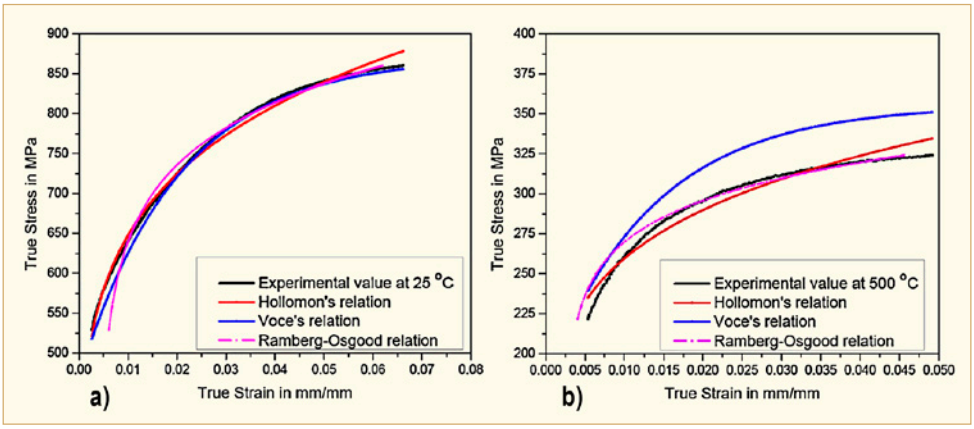

Figure 4-2: Fit of true-stress—true-strain data for Zr-2.5Nb to equations of [Hollomon, 1945], [Voce, 1947/8] and [Ramberg & Osgood, 1943] at test temperatures of (a) 25 and (b) 500°C [Dureja et al, 2014].

The mechanical properties of Zr-2.5Nb pressure tubes can be affected by the number of times the ingot is melted, either twice or four times (see ZIRAT20/IZNA15 Special Topic Report on Microstructure of Zirconium Alloys and Effect on Performance, Section 5.1), and by position with respect to the extrusion end. In the CANDU version of cold-worked Zr-2.5Nb, the tubes are cold-worked about 27% after extrusion at 815°C. The part of the tube that exits the extrusion press first is called the front end and it tends to be slightly weaker than the back end that exits the extrusion press last; at room temperature in the hoop direction the mean 0.2% yield strength for front ends is about 782 MPa while that of the back ends is 803 MPa. The few degrees lower temperature of the final part of the extrusion leads to a measurably lower grain width at the back end compared with the front end: 0.34±0.06 μm vs. 0.45±0.08 μm [Griffiths et al, 2002]. In the Indian version, the tubes are cold-worked in two stages: 50 to 55%, annealed at 550°C for 6 h, then cold-worked a further 20 to 25%. Tensile tests in the temperature range 25 to 450°C on four tubes show that the back end of the tubes is a little stronger than the front end, Figure 4-3, but the work hardening coefficients, h in Eq. 4-2, are similar and slightly larger than in CANDU tubes, Figure 4-4 [Khandelwal et al, 2015] but much lower than reported by [Dureja et al, 2014] on similar tubes. The number of melts does not affect the tensile behaviour, Figure 4-5. The concentration of oxygen, an important strengthening element, was similar in each tube, 1050 to 1290 ppm, while the concentration of Fe was 1100 to1200 ppm in the double melted tube, about twice that in the quadruple melted tubes. The concentration of Cl was much lower in the quadruple melted material than in the double melted material: 0.19 to 0.83 ppm vs. 2.4 ppm. Neither of these low concentrations of Cl has any effect on strength nor plasticity but the higher value in the double melted material is sufficient to greatly reduce the crack growth resistance, dJ/da, Figure 4-6. This strong effect of Cl on crack growth resistance was first observed in CANDU pressure tubes leading to the recommendation for quadruple melting [Theaker et al, 1994].

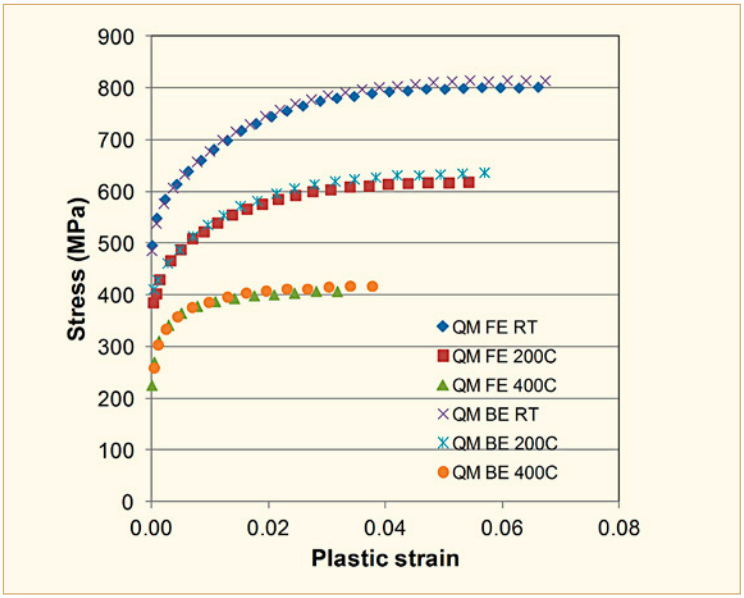

Figure 4-3: Tensile curves for Zr-2.5Nb pressure tubes showing that back ends, BE, are slightly stronger than front ends, FE, based on [Khandelwal et al, 2015].

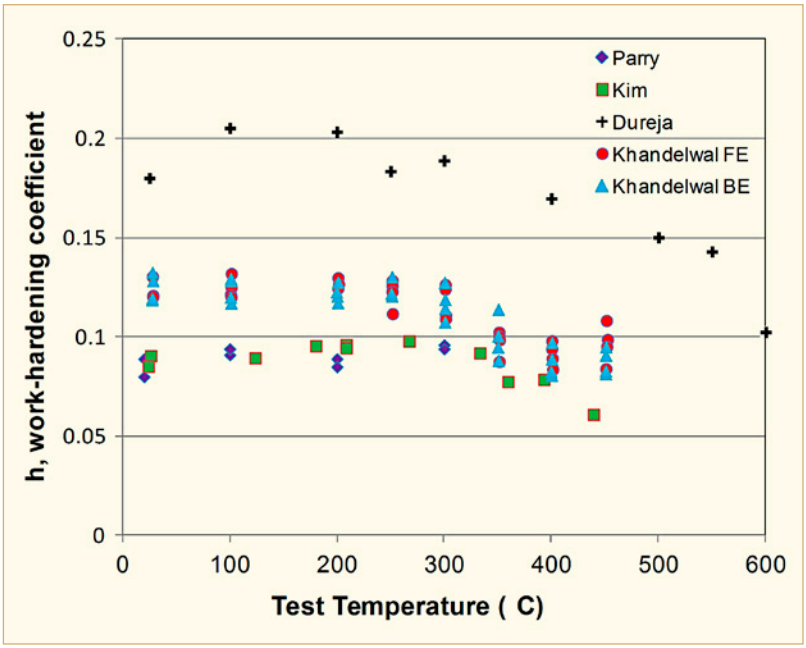

Figure 4-4: Effect of temperature on h, the work-hardening coefficient, of Zr-2.5Nb material showing no effect of position in pressure tube, front end (FE) vs. back end (BE) and similarity between some Indian and CANDU material, based on [Khandelwal et al, 2015], [Dureja et al, 2014], [Kim, 2008a] and [Parry, 1966].

5 Dimensional stability (Ron Adamson)

5.1 Introduction

This topic covers changes in dimensions experienced by reactor bundle components during service. The component designer must be able to quantify the expected changes from the as-fabricated design as a function of time, neutron fluence, and component exposure or burnup. It is not unusual for the long Zircaloy reactor components (fuel tubes, water rods, guide tubes, channels) to increase in length by 40 mm or more during normal service. A major complication arises when, as is usual, the change in dimension is not uniform in a component or collections of components, resulting in bending and/or increase in local stresses. An example is the case of BWR channels that have experienced severe bending (enough to interfere with smooth control blade motion) due to side-to-side differential lengthening resulting from neutron flux gradients and build-up of differential hydrogen/hydride concentrations (covered in detail in [Garzarolli et al, 2011]).

The primary drivers of dimensional stability (or more relevant, dimensional instability) are

1) thermal expansion, unavoidable due to

- different thermal expansion coefficients for different materials
- temperature gradients as a function of both time and location

2) irradiation growth

- a function material, microstructure, neutron fluence, texture, temperature
- not a function of stress
- reviewed in detail by Adamson, Section 5, “Irradiation Growth,” [Rudling et al, 2012]
- strongly related to irradiation-induced changes in microstructure and microchemistry

3) irradiation creep

- a function of stress, material, neutron flux, texture, temperature, time or neutron fluence
- reviewed in detail in [Adamson et al, 2009a],
- sources of stress are
  - differential pressure inside and outside fuel tube
  - pellet cladding mechanical interactions (PCMI), due to fuel expansion during power cycles or excursions
  - differential dimensional changes of linked components
  - corrosion buildup in tight spaces like crevices

4) hydrogen and/or hydride concentration

- due to normal or shadow corrosion
- dimensional strain induced by
  - volume change larger than that for zirconium

  - effect on magnitude of irradiation growth
  - reviewed in many ZIRAT reports including in [Garzarolli et al, 2011].

Measurement of dimensions and material characteristics are accomplished through

- poolside examinations of bundles and components, as described in [Rudling & Patterson, 2009] For example, fuel rod, channel or guide tube lengths can routinely be viewed and measured by standard poolside equipment.
- hot cell examinations
- requires shipment of radioactive material to a hot cell in the U.S., Europe, Russia or Canada.
  - This procedure is expensive and the choice of hot cell facilities is very limited.
  - Examinations are summarized in ZIRAT19STR, [Mahmood et al, 2014] and in a follow-on STR in 2016.
- Specially designed experiments
  - In-reactor experiments are described in many ZIRAT STRs and regularly in journals such as the Journal of Nuclear Material and special books such as the series of Zirconium in the Nuclear Industry symposiums. All such experiments involve shipping radioactive material to hot cells and special radioactive material laboratories.
  - Charged particle bombardment experiments are conducted using ion accelerators of various kinds throughout the world. Advantages include simulating neutron irradiation in significantly less time than in reactors and producing material with significantly lower radioactivity than in reactors. However, significant disadvantages include providing irradiation damage in only thin layers (micrometers thick) and uncertainties in whether the high rates of damage and physical details of damage actually do simulate reactor neutron irradiation. However, use of and understanding of changed particle irradiation is increasing in the zirconium alloy field. A review of the topic is [Adamson, 2014]. Another review, an excellent recent one, is [Yan et al, 2015a].

This ZIRAT20 AR review of Dimensional Stability (DS) includes

- irradiation-induced microstructural changes relevant to DS,
- recent literature publications on DS topics.

5.2 Review

[Choi & Kim, 2013] published a well-rounded review of radiation – induced dislocation and growth phenomena, including an extensive reference list. Experimental data and model/theoretical analyses were presented. The usual parameters affecting growth were briefly examined, including texture, temperature, grain size, point defect trapping, vacancy and interstitial mobility, intern-granular stresses, anisotropic diffusion, and production bias modelling. Data from [Gilbert et al, 1979] and [Kelly & Blake, 1973] also were included. Choi and Kim indicate that the nature of <a> component dislocation loops (a-loops) changes with irradiation temperature. The ratio of vacancy character to interstitial character of the a-loops is given: 50% vacancy for 350°C (623K) and 70% vacancy at 390°C (673K).

Choi and Kim also claim that for low irradiation temperature (<300°C [573K]), the a-loops are all or predominantly interstitial character. This is contradicted by the data of [Griffiths, 1988] that indicated annealed Zr irradiated to 1.3×10^{21} n/cm^2 at 300°C (573K) had approximately equal numbers of vacancy and interstitial loops. In addition, a-loops in Zircaloy-4 irradiated at 307°C (580K) to 8×10^{21} n/cm^2 were 68% vacancy type. Annealing this material at 500°C (773K) resulted in larger a-loops, but still mostly vacancy in type. Interestingly, a-loops in Zircaloy-2 irradiated at 57°C (330K) were too small to analyse; however, after annealing at 500°C (773K) the loops were larger, and predominately interstitial in type [Griffiths, 1988]. This provides a hint that at low temperature where vacancies are not mobile, interstitial type loops predominate. It is also known that for 80°C (353K) irradiation temperature, <c> loops do not form [Rogerson, 1988]. This has important significance for detailed growth modelling, as in [Christensen et al, 2015], and [Golubov et al, 2015].

5.3 Microchemistry

As discussed in many previous reports, both neutron irradiation and charged particle bombardment (see [Adamson, 2014]) result in disbursement of alloying elements into the Zr matrix. In the Zircaloys, Fe, Ni and, to a lesser extent, Cr dissolve from SPPs as shown by EDX (energy dispersive X-ray spectroscopy). However, determination of the location of the solute atoms or clusters is beyond the capability of current TEM technology. Of the new modern detection techniques, 3-D atom probe or atom probe tomography (APT) is increasingly being applied to solve this mystery. Using laser pulsing and enhanced analytical capability, along with modern FIB (field ion bombardment) specimen preparation technologies, three dimensional images of many millions of element-identified atoms can be obtained for, small (e.g., $50 \times 50 \times 140$ nm^3) volumes of material in selected regions of a specimen. (Note that "small" is really small, much smaller than the metal grain size and about the size of a small SPP found in the zirconium alloy.) Thus far, APT has been aimed mainly at studying details of corrosion and hydrogen pickup phenomena ([Dong et al, 2013]; [Hudson & Smith, 2009]; [Sundell et al, 2012]; [Tejland et al, 2011]; several programs within EPRI/NFIR; and references found therein). Those papers, all describing unirradiated Zircaloy, observed segregation of Fe and/or Ni at grain boundaries in both the metal and oxide (Figure 5-1 and Figure 5-2).

[Sundell et al, 2012] hypothesize that 1) dislocations form on the metal side of the metal/oxide boundary due to stresses induced by the oxidation process, 2) these dislocations "attract" mobile Fe and Ni atoms and 3) the decorated dislocations are incorporated into the growing oxide front, and thus can extend from the metal into the oxide.

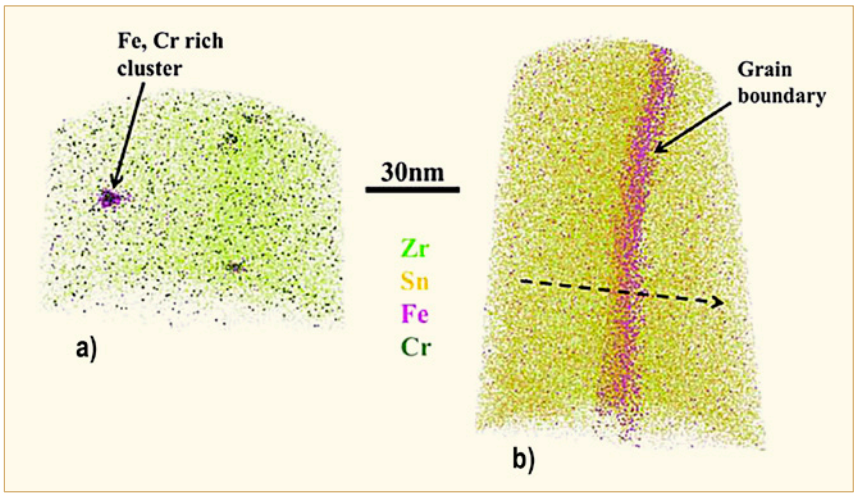

Figure 5-1: Bulk Zircaloy–4: (a) APT reconstruction showing Fe, Cr rich clusters; (b) APT reconstruction showing grain boundary with Fe and Sn segregations [Dong et al, 2013].

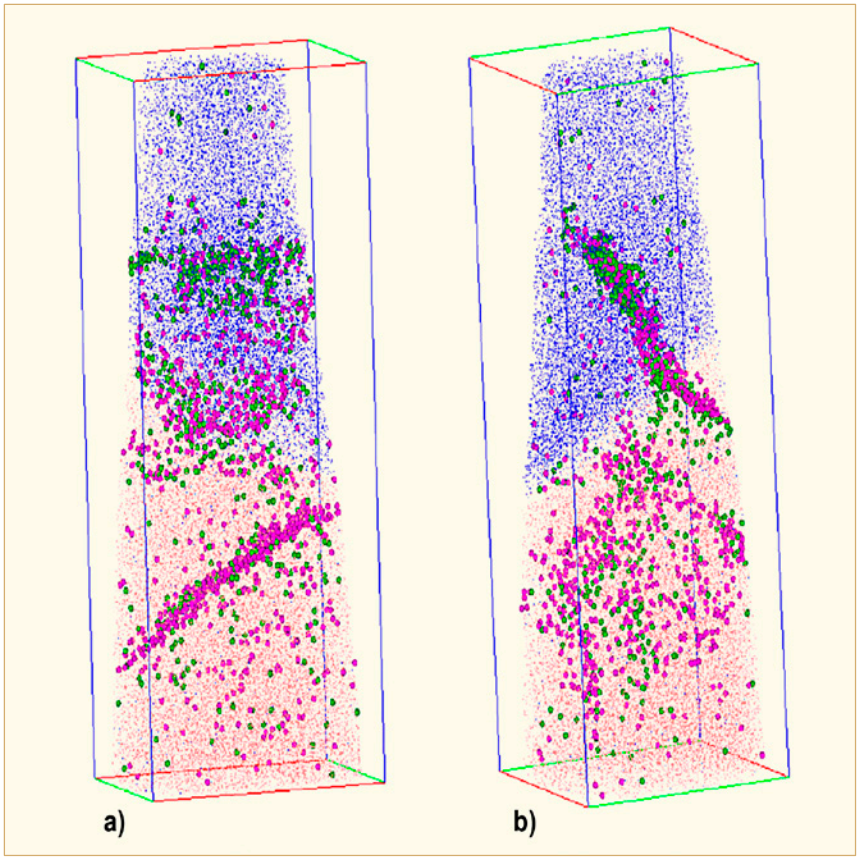

Figure 5-2: Segregation of Ni (green) and Fe (purple) in the Zircaloy-2 metal (orange) and in the ZrO_2 scale (blue). The size of the box is 50 × 50 × 140 nm^3 [Sundell et al, 2012].

Of particular interest for irradiation growth is the paper by [Sundell et al, 2014], who used APT to study irradiated Zircaloy-2, the same material used in the extensive work reported on this high fluence (16×10^{25} n/m^2, E > 1 MeV) cladding [Valizadeh et al, 2010]. The areas examined are close to the metal/oxide interface that likely contain high concentrations of hydrogen/hydride; it is unclear how this affects the analysis. The results are new and interesting:

- Some portions of the metal have a dense distribution of Fe and Cr-rich clusters having size in the 1-5 nm range. It is hypothesized that the clusters are associated with <a>-component dislocation loops (a-loops) known to have been formed during irradiation. Figure 5-3 gives the images. Note that Fe and Cr clusters apparently are absent in the right side grain, where only Sn is clustered. Also, little Ni was found in the analysed specimens.

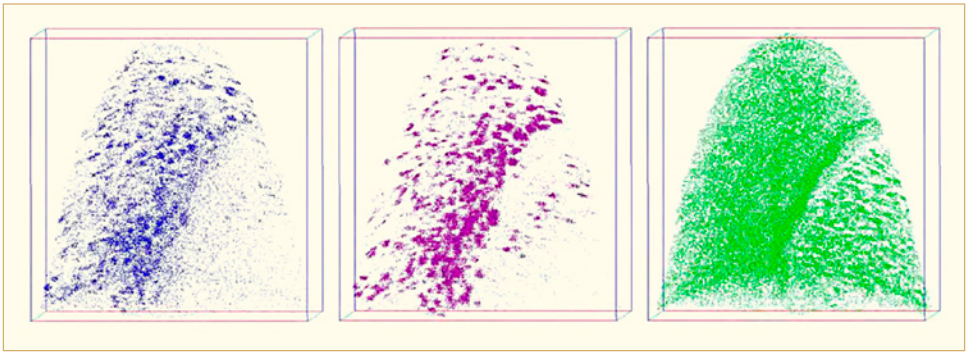

Figure 5-3: Distribution of Fe atoms (blue), Cr atoms (purple) and Sn atoms (green) in two adjacent grains in the Zr metal. The box is 140 × 140 × 140 nm^3 [Sundell et al, 2014].

6 Corrosion and Hydriding (Friedrich Garzarolli)

6.1 Recent publications on mechanistic studies

Uniform corrosion of Zr alloys in water and steam proceeds by a cyclic mode, exhibiting in most cases a cyclic rate transitions after certain time-, respectively, oxide thickness-intervals, ~2 µm. There is still no generally accepted root cause model for the cyclic corrosion rate transition. Several different mechanisms are proposed from different examinations. The corrosion behaviour of Zr-alloys in high pressure water and steam is out of reactor governed by the following mechanistic aspects:

1) The average thickness and quality of the inner dense layer, often called barrier layer.

2) The oxide structure that forms on the metal/oxide interface (nucleation of new e.g. tetragonal grains or growth of monoclinic columnar grains[3]). The shape of the oxide grains within the barrier layer can be long columnar (normal corrosion), short columnar (moderate accelerated), or equiaxed (nodular corrosion) and depends on the Zr-oxide grain nucleation at the metal/oxide (M/O) interface. Monoclinic ZrO_2 has a high surface energy, but OH^- and H^+ can significantly reduce the surface energy (by reaction with the free bonds at the GB surface) and affect nucleation resulting in shorter columnar grains or even in small equiaxed moclinic grains. Their size and shape affects the diffusion of O-ion-vacancies (which proceeds preferentially via grain boundaries) as well as the tendency to crack, governing the average barrier layer thickness.

3) The content of dissolved alloying elements, which may concentrate at the oxide grain boundaries (e.g. Sn) and affect their properties (diffusion of O-ion-vacancies) or decrease the electronic resistance of the barrier layer (e.g. Nb).

4) The content, type, and size of SPP, that may affect the electronic resistance of the barrier layer and delay or even accelerate pore/crack formation (rate transition) in the outer part of the barrier layer as consequence the volume increase connected with their delayed oxidization in the outer part of the barrier layer.

5) The stress in the oxide, created by the oxidation induced volume increase (56%), which results normally mostly in thickness stretching and only ~1% of the volume change (depending on the oxide layer texture) leads to an increased crosswise growth, e.g. [Parise et al, 1998]) and is limited by the yield strength or creep resistance (at ≥400°C) of the under-laying Zr-alloy metal.

6) At oxide thickness before the cyclic transition the electronic resistance of the oxide layer and consequently the potential gradient increases resulting in a higher HPUF and a higher H content at the O/M interface [Harada & Wakamatsu, 2007]. Zry-alloys with a high Sn and low Fe content exhibit under cathodic polarization a significant increase of corrosion and hydrogen pickup (HPU), whereas Zr-Nb alloys having a relatively high electric conductivity show only little effect of polarization on HPU [Bauer et al, 2000].

7) LiOH additions to the water and certain impurities cause an increased corrosion above a critical conncentration (in case of LiOH probably due to the increasing solubility of ZrO_2 with increasing pH [Cox & Wu, 1993] and [Kritzky et al, 1997]).

[3] If new very fine oxide grains are formed or the compressive stress at the M/O is very high the initial grains are tetragonal, which recrystallize to monoclinic ZrO_2, what is the normal oxide structure in the temperature range of interest.

[Shevyakov et al, 2013] examined the structure of the oxide layers formed on the Russian alloys E110 and E365 after corrosion in 360°C water for 50–600 days (1–15 μm) by TEM examination. They reported (Figure 6-1) fine (5–10 nm) tetragonal oxide grains close to the M/O interface and a transition to columnar monoclinic ZrO_2 grains occurring gradually, with increasing distance from the interface. The transverse size of the monoclinic phase grains is 20–60 nm in case of E110 and 10–40 nm in case of E365. The tetragonal grains, which are oriented in the direction of $(110)_{tetra}$ parallel to the M/O-interface, begin to grow and get a columnar structure. The β-Nb precipitates in E110, are still metallic at the O/M interface but become amorphous, starting at a distance of >300 nm (from the OD) to a fully amorphous state (oxidized) at >1500 nm. In case of the $Zr(NbFe)_2$ precipitates in E635 amorphization begins at >100 nm from the M/O-interface and becomes complete at 600–700 nm.

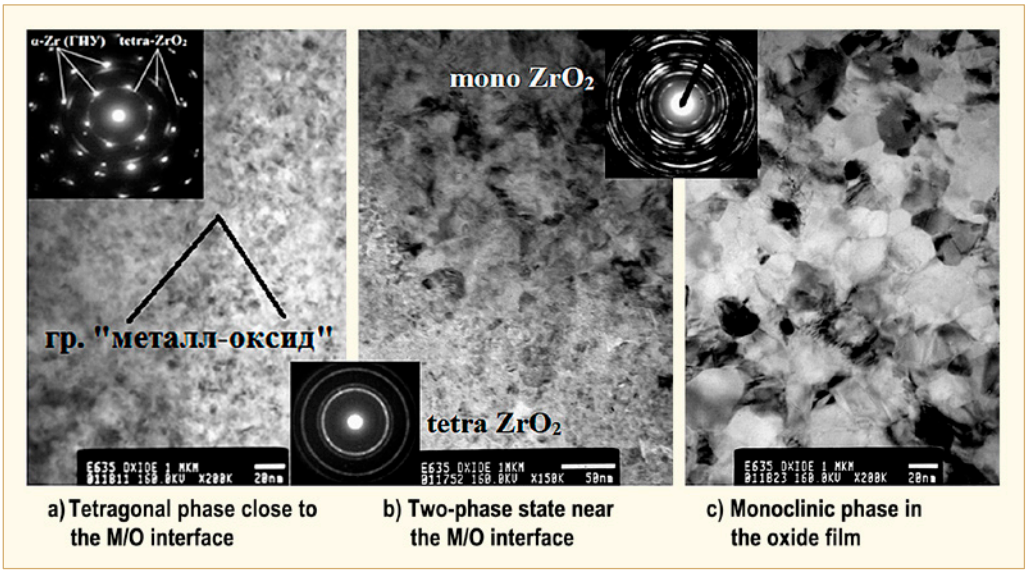

Figure 6-1: TEM figures taken parallel to the oxide growth front revealing a tetragonal layer close to the O/M interface that transforms to monoclinic ZrO_2 phase occurring gradually, with increasing distance from the interface in the oxide film formed in 360°C water on E636 [Shevyakov et al, 2013].

In the last years several reports considered the formation of tangential cracks at the transition in the oxide at the meal-oxide interface, above peaks in the in the interface roughness, as an important aspect. It was, however not fully clear, whether these cracks form immediately before the transition or were formed during the fast corrosion period after the transition.

Several papers on the mechanism of out reactor corrosion of Zircaloy-4, ZIRLO, and Zr1Nb0.1Fe (A-0%Sn) were reported by scientists of the Universities of Manchester and Oxford.

[Platt et al, 2015] presented a detailed analysis of the development of interface profile at the metal-oxide interface (roughness and lateral cracks) for samples of the tree alloys exhibiting a corrosion behaviour, as shown in Figure 6-2.

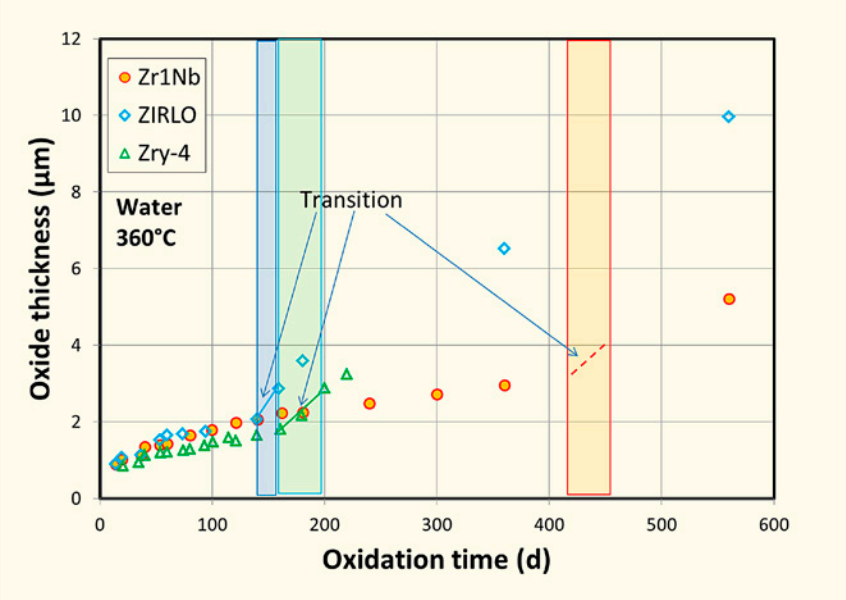

Figure 6-2: Oxidation kinetics of recrystallized Zircaloy-4, ZIRLO and Zr1Nb0.1Fe in 360°C water, data from [Platt et al, 2015] and [Garner et al, 2015c].

Figure 6-3 shows the shape of metal/oxide (M/O) interlayer and the observed micro-cracks in the oxide layer on ZIRLO showing isolated cracks forming early on (80 days) but becoming more frequent and apparently interconnected just before the transition (140 days). After the rapid oxidation, post-transition (160 days) these cracks have formed a layer. The Zry-4 samples showed a similar micro cracks before, at, and after the transition. Zr1Nb0.1Fe, which was also examined after 80, 140 and 160 days (all before transition) showed only spare and not interconnected cracks at the M/O interface.

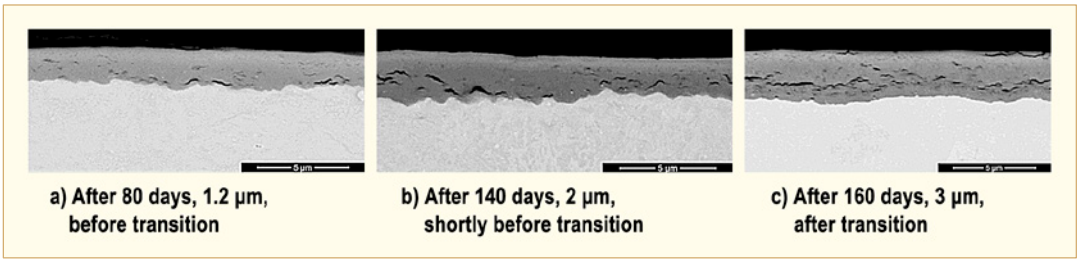

Figure 6-3: SEM cross section images of ZIRLO samples with different oxide layers, [Platt et al, 2015].

In a later publication [Hu et al, 2015] the same group of scientists reported on the cracking behaviour of Zr1Nb0.1Fe at the O/M interface (Figure 6-4), and showed that even after 225 d (2 µm) and 360 d (3 µm) of oxidation a pre-transition characteristics was seen and that post-transition characteristics was seen only after 585 d exposure (5.4 µm) revealing two distinct layers of cracks parallel to the O/M interface. The two layers are not exactly parallel suggesting that the local transition happens at different times in different locations.

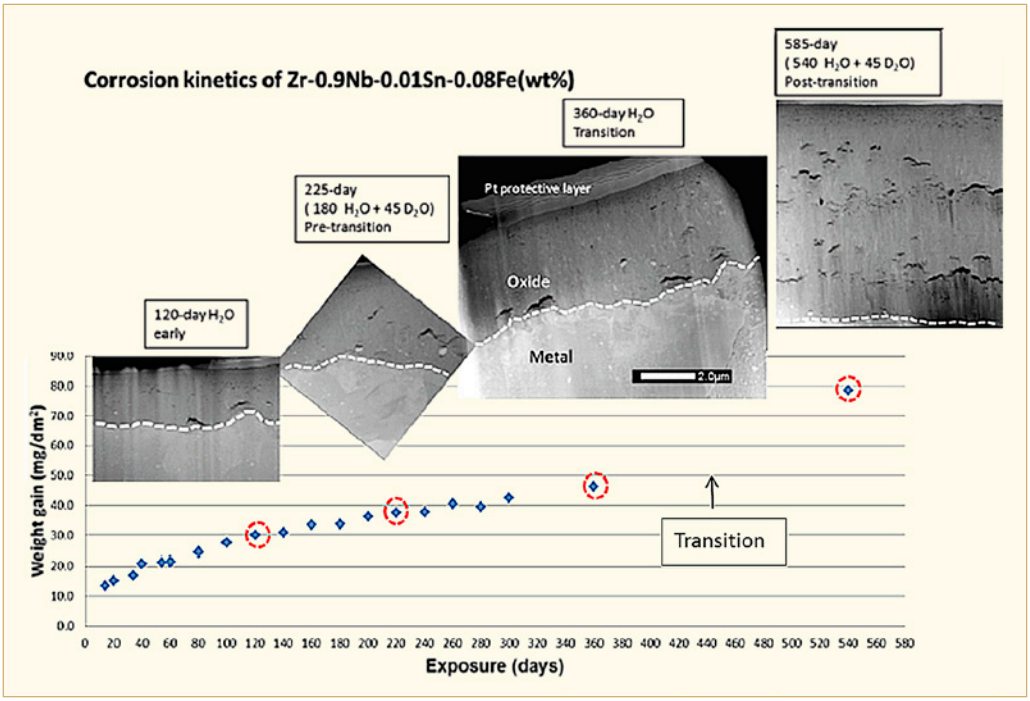

Figure 6-4: SEM cross section images of Zr1Nb0.1Fe (A-0%Sn) samples with different oxide layers, [Hu et al, 2015].

In the study of [Platt et al, 2015] the roughness of the O/M interface was analysed versus the oxidation time. The root mean square (R_{dq}) of the interface slope, taking into account the amplitude and the wavelength, was estimated via the oxidation time (Figure 6-5 for Zircaloy-4), for the median of 100 images. The scatter bars represent the upper and lower quartiles. The yellow highlighted region represents the time frame in which transition is predicted to have occurred. The figure shows an increase of R_{dq} up to 160 days, i.e. just before transition. After start of transition (increased corrosion) a reduction in the interface roughness occurs and afterwards it increases again. The number of micro-cracks in the oxide increases at the start of transition and consequently also the average oxygen diffusion rate and the corrosion rate. Finite element analysis of the tetragonal to monoclinic phase transformation has shown that the formation and growth of lateral cracks should locally destabilize the tetragonal phase potentially leading to the formation of nano-scale cracks and pores. This would create fast ingress routes for oxygen containing species. At 180 days oxidation, i.e. the fast corrosion period after transition, the scatter becomes very high, indicating that some regions of the oxide have gone through transition, whereas other regions have not.

7 Primary failure and secondary degradation – open literature data (Peter Rudling)

The open literature data are provided in the following sections.

7.1 Introduction

7.1.1 Primary failures

During reactor operation, the FR may fail due to a primary cause such as fretting, PCI manufacturing defects, corrosion, etc. (Table 7-1).

Table 7-1: Primary failure causes for LWR fuel during normal operation and Anticipated Operational Occurrences (AOO).

Primary failure cause	Short description
Excessive corrosion	An accelerated corrosion process results in cladding perforation. This corrosion acceleration can be generated by e.g., CRUD deposition (CILC)[a], Enhanced Spacer Shadow Corrosion, (ESSC)[b], (in BWRs), dry-out due to excessive FR bowing.
Localised hydriding	Fuel may fail in hydrided regions fractured under tensile loading that arose with accumulation of exposure during the course of normal operation (BWRs)[c]. Li seems to be involved in the failure mechanism (It is not clear from where the Li originated since Li does not normally occur in BWR coolants). More work is needed to understand the mechanism that led to the localised hydriding.
Manufacturing defects	Non-through-wall cracks in the fuel cladding developed during the cladding manufacturing process. Defects in bottom and/or top end plug welds. Primary hydriding due to moisture in fuel pellets and or contamination of clad inner surface by moister or organics. Too large a gap between the FR and the spacer grid supports (poor spacer grid manufacturing process) leading to excessive vibrations in PWR fuel causing fretting failures. Chipped pellets may result in PCI failures both in liner and non-liner fuel.
PCI	PCI – an iodine assisted SCC phenomenon that may result in fuel failures during rapid power increases in a FR. There are three components that must occur simultaneously to induce PCI and they are: 1) tensile stresses—induced by the power ramp, 2) access to freshly released iodine-occurs during the power ramp, provided that the fuel pellet temperature becomes large enough and 3) a sensitised material—Zircaloy is normally sensitive enough for iodine stress-corrosion cracking even in an unirradiated state.
Cladding collapse	This failure mechanism occurred due to pellet densification. This failure mode has today been eliminated by fuel design changes and improved manufacturing control.
Fretting	This failure mode has occurred due to: Debris fretting in BWR and PWR. Grid-rod fretting – Excessive vibrations in the PWR FR causing fuel failures. This situation may occur for example due to different pressure drops in adjacent FAs causing cross-flow. Baffle jetting failures in PWRs – Related to unexpectedly high coolant cross-flows close to baffle joints.

[a] CILC – an accelerated form of corrosion that has historically resulted in a large number of failures in BWRs. Three parameters are involved in this corrosion phenomenon, namely: 1) Large Cu coolant concentrations as a result of e.g., aluminium brass condenser tubes, 2) Low initial fuel rod surface heat flux – occurs in Gd rods and 3) Fuel cladding that shows large initial corrosion rates- occurs in cladding with low resistance towards nodular corrosion.

[b] This corrosion phenomenon resulted in a few failed rods. The mechanism is not clear but seems to be related to galvanic corrosion. This corrosion type may occur on the fuel cladding in contact or adjacent to a dissimilar material such as Inconel. Thus, this accelerated type of corrosion occurred on the fuel cladding material at spacer locations (the spacer springs in alloy BWR fuel vendors fuel are made of Inconel). Water chemistry seems also to play a role if the fuel cladding material microstructure is such that the corrosion performance is poor. Specifically coolant chemistry with low Fe/(Ni±Zn) ratio seems to be aggressive (provided that the cladding material shows poor corrosion performance. A fuel cladding material with good corrosion resistance does not result in ESSC, even in aggressive water chemistry.

[c] Sixty-three GE13B 9×9 fuel assemblies in Browns Ferry, Unit 2 (BF2) during Cycle 12 failed. Seven rods were examined in hot cell to determine the primary failures cause.

ANT International, 2014

Table 7-2 and Table 7-3 provide key data for some of the most recent fuel-failure cases.

Table 7-2: Summary of previous PWR/PHWR failure key events, see previous ZIRAT/IZNA-reports for details. New results added to the table from the ZIRAT18/IZNA13 AR [Rudling et al, 2013] is in red text.

Nuclear unit	Type of primary failure	Comment
TMI-1, Cy 10, 1995	Nine high peaking FRs, Zry-4 Cladding, failed after 122 days of operation. CRUD/corrosion related failures.	All failed and degraded pins reportedly had Distinctive CRUD Pattern (DCP)[4]. High peaking factors, thermal-hydraulic conditions. Calculations indicated that no boiling should have occurred on the pins with DCP, although the pins with DCP were calculated to have a slightly higher temperature. Water chemistry (low pH at BOC, pH < 6.9, max LiOH 2.2 ppm). Some, AOA effect was found reaching a maximum in the middle of cycle 10. The source of the CRUD could not be determined. The CRUD sampling showed that the nickel-to iron ratio was in the range 1.25 to 16.7, which was reportedly somewhat lower than in previous investigations.
Seabrook, Cy 5, 1997	Five one-cycle ZIRLO rods failed. CRUD/corrosion related failures.	Longer cycle in transition to 24-month cycle. Possibly CRUD-induced overheating resulting in substantial nucleate boiling.
EdF data reported in 2009 [Thibault et al, 2009]	The main failure causes in the EdF plants are: GTRF wear, Clad manufacturing defects and, Excessive fuel assembly bowing (resulting in assemblies grids hanging-up during loading and unloading and IRI)	A significant number of fuel failures were related to the M5 fuel cladding in 1300 MWe and 1450 MWe units. The M5 FR failures were due to fabrication defects either related to the end plug girth or fill hole weld or defects in the fuel clad itself at grid levels (related to the pulling of the rods into the assembly structure). To resolve these manufacturing issues, AREVA has modified the welding techniques as well as the rod pulling procedure. It was observed that there were no GTRF failures in 2008 (in previous years there have always been some GTRF failures). The reasons for the great improvement is thought to be due to that both AREVA and Westinghouse have introduction reinforced FAs design (AFA3GLr – AREVA and RFA2- Westinghouse). Since the introduction of the AREVA AFA3G design in 1999, a decrease of the average core bow in EdF NPPs has been observed, especially on the 900 MW units, but not as fast as expected. The maximum values of bowing remain relatively high on the 1300 MW units, typically between 15 and 19 mm for a “S shape” bow. The Westinghouse RFA fuel design behaves in the same way with similar bowing range while HTP assembly deformations are twice less. Incomplete Rod Insertions (IRIs) due to bowing have been significantly reduced since the AFA3G FA’s design has been loaded in EdF NPPs and despite the increasing of the average discharge burnup of the FAs. In 2008, no anomaly of RCCA drop time was observed in EdF NPPs during the BOC tests. Concerning the EOC tests, no anomaly was observed in the 12 feet units whereas four RCCAs dropped without recoil in the 14 feet units. Three of them was AFA3G FAs (two “2nd cycle” FAs and one “4th cycle” FA) and one was the older design (AFA2G). The number of FAs damaged during handling operations has decreased in 2008 but remains significant. The damages concern only AFA 2G or 3G design and mainly the 14 feet units. It occurs during the unloading operations. The damages generally occur during a “three-sided box” extraction and result from grids’ hanging due to bowing and to a reduced gap between FAs following unexpected grid growth due to re-crystallized Zircaloy-4.

[4] This acronym implies that the fuel inspection revealed CRUD deposits on the fuel rod and that the deposits were uneven in the rod circumference.

8 LOCA, RIA, Seismic event (Peter Rudling)

8.1 Introduction

8.1.1 Seismic event

To assure safe operation following a seismic event, additional criteria are defined. Two levels of ground motion excitation, corresponding to two earthquake levels, are defined for safety-related structures, systems, and components in operating nuclear power plants. Compliance with specified criteria assure that plant safely is maintained following each event.

For the first-level earthquake, the Operating Basis Earthquake (OBE), the load factors and acceptable allowable stresses ensure that the stresses in plant structures remain at least 40 percent below the yield stress of the material for the event.

For the second-level earthquake, the Safe Shutdown Earthquake (SSE), whose vibratory motion is usually twice that of the OBE), the associated load factors and allowable stresses ensure that the stresses in the plant structure and assembly remain close to the yield stress of the specific materials; a small excursion in the inelastic range is allowed when the SSE load is combined with accident loads, usually those associated with a LOCA event.

The following criteria relates to a seismic event:

- OBE-Allow continued safe operation of the FA following an OBE event by establishing that the FA components do not violate their dimensional requirements. This is most simply assured by requiring that the stresses in components remain below the yield stress of the unirradiated components.
- SSE-Ensure safe shutdown of the reactor by maintaining the overall structural integrity of the fuel assemblies, control rod insertability and a coolable geometry within the deformation limits consistent with the ECCS and safety analysis. Requirements to assure safe shutdown are:
  - Fuel rod or assembly fragmentation does not occur due to seismic loads.
  - Control rod insertability is maintained by confirming no or small plastic deformation of components.
    - Adequate static and dynamic crush strength of the spacer assembly (PWR/VVER) and fuel channel (BWR), including requirements for Condition III and IV accidents must be ensured. The grid should maintain the fuel rods in a coolable configuration. The seismic criteria are particularly critical since the PWR/VVER spacers and BWR fuel channels absorb the lateral seismic shocks. This means that the hydrogen content in the Zr alloy spacer (PWR/VVER) and fuel channel (BWR) should be limited.
  - Confirmation that the FA (top and bottom nozzles) maintains engagement with the reactor internals.

  To ensure that the criteria above are met, fuel vendors limit the maximum allowable amount of hydrogen in grids (for PWRs/VVERs) and fuel channels (for BWRs) to limit the hydrogen embrittlement effect (Figure 8-1). If the hydrogen content becomes too large in these components, the grids or the fuel channel may fracture due to the seismic load making it difficult to insert the control rods and shut down the reactor.

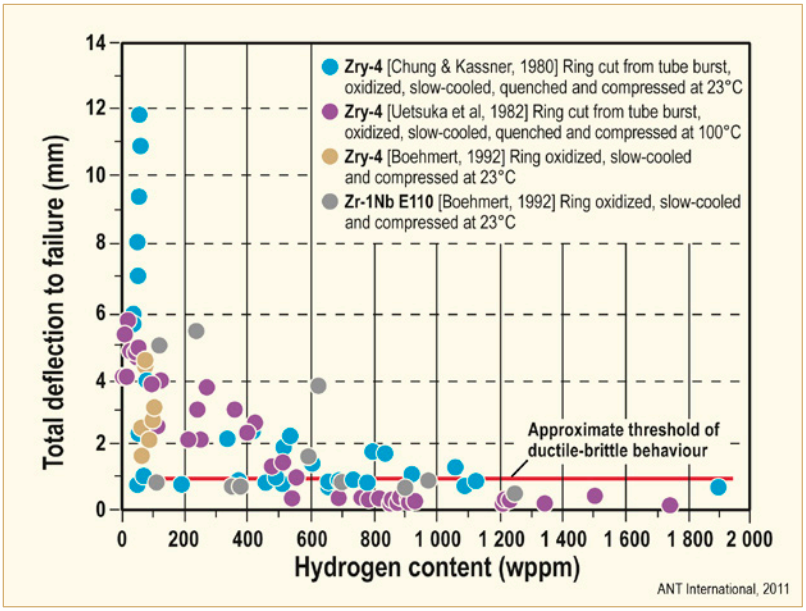

Figure 8-1: Effect of hydrogen on ring compression ductility of unirradiated samples prehydrided before RCT, after [Chung et al, 2001].

Increased burnup may lead to additional HPU through Zr-alloy corrosion of the grids (for PWRs/VVERs) and fuel channels (for BWRs) which may reduce the margins towards satisfactory performance of these components during the seismic event.

8.1.2 Loss of Coolant Accident

The design basis Loss of Coolant Accident (LOCA) is a break in a pipe that provides cooling water to the reactor vessel. Analyses are performed for a variety of break sizes and locations to demonstrate that the ECCS can maintain the fuel in a coolable geometry. The limiting break is typically in one of the cold, main coolant pipes of a PWR or one of the intake pipes to the recirculation pump of a BWR.

The LOCA process starts by the decrease and ultimate loss of coolant flow at the same time that the reactor is depressurized (Figure 8-2). The loss of coolant flow decreases heat removal from the fuel, increasing the fuel temperature and causing a significant temperature rise of the cladding. The decrease in system pressure causes an outward pressure differential and a hoop stress in the cladding wall. The result is the plastic deformation, or *ballooning* of the cladding. Ballooning may also result in *fuel relocation*[6] that may impact the cladding temperature as well as the Equivalent Cladding Reacted (ECR[7]) in the later phase of LOCA.

Ballooning of the fuel rods may result in *blockage* of the coolant sub-channel that in turn may impact the fuel coolability. If large fuel clad burst strains occur at the same axial elevation, *co-planar deformation*, in the FA, the coolability may be significantly degraded. Specifically, the clad azimuthal temperature gradient will strongly impact the burst strain. The extent of the ballooning is also dependent on:

[6] Fuel relocation may occur, if during LOCA a section of the fuel rod experiences ballooning, by slumping of fuel fragments from upper location in the ballooned section.
[7] The ECR is defined as the total thickness of cladding that would be converted to stoichiometric ZrO_2 from all the oxygen that are contained in the fuel cladding as ZrO_2, and oxygen in solid solution in the remaining clad metal phase.

- Creep strength of the cladding.
- Stress in the cladding and the corresponding strain rate.
- Temperature and the rate of temperature increase.

Depending on the temperature, the cladding ductility and the rod internal pressure, the cladding will either stay intact or may burst which will allow steam to oxidize the fuel clad inner surface. In addition, some of the hydrogen released by the water/zirconium corrosion reaction inside the burst fuel may be picked up by the cladding resulting in very high local hydrogen concentrations (1000-3000 wtppm H). A fuel cladding with such high hydrogen concentrations will be very brittle even though the cladding is not oxidised at all, i.e. ECR is 0. The fuel clad axial temperature distribution will determine the axial elevation of the ballooned and burst fuel rods in the assembly. The axial and azimuthal fuel clad temperature distribution is a result of the heat transfer mechanisms at the surfaces of the cladding.

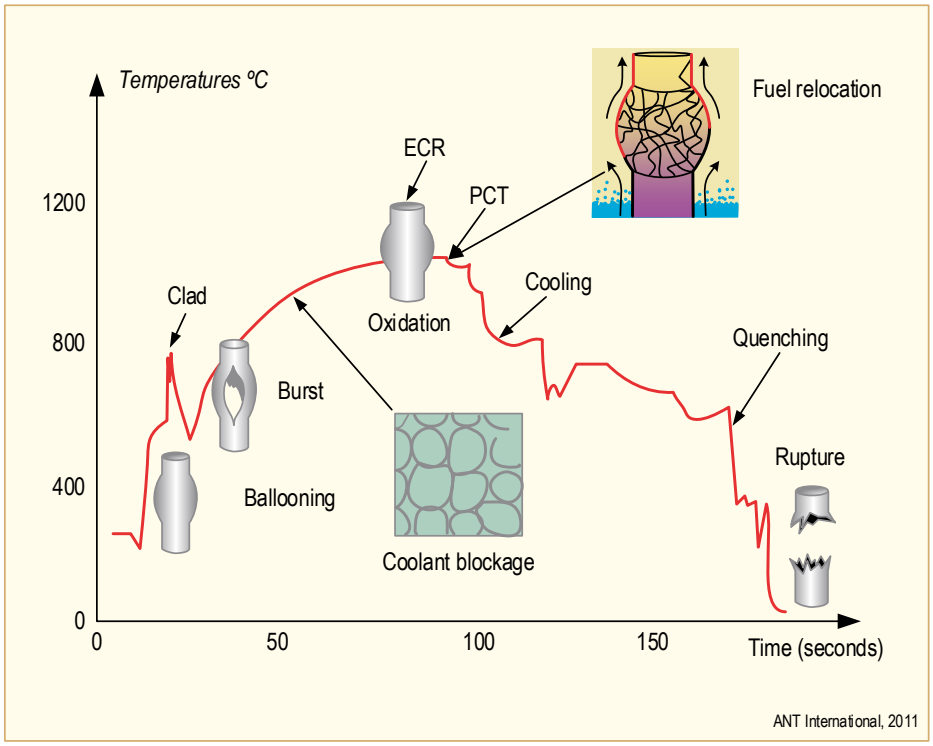

Figure 8-2: Typical LOCA in a PWR.

The increasing temperatures and presence of steam will cause the intact cladding to oxidize on the OD and the burst cladding to oxidize on both the OD and ID (two sided oxidation) until the ECCS is activated and the water quenches the cladding. The oxidation process at the high LOCA temperatures will increase the oxygen and hydrogen content in the cladding, reducing its ductility and resistance to rupture. The process and final structure of the cladding after a LOCA cycle is shown in Figure 8-3.

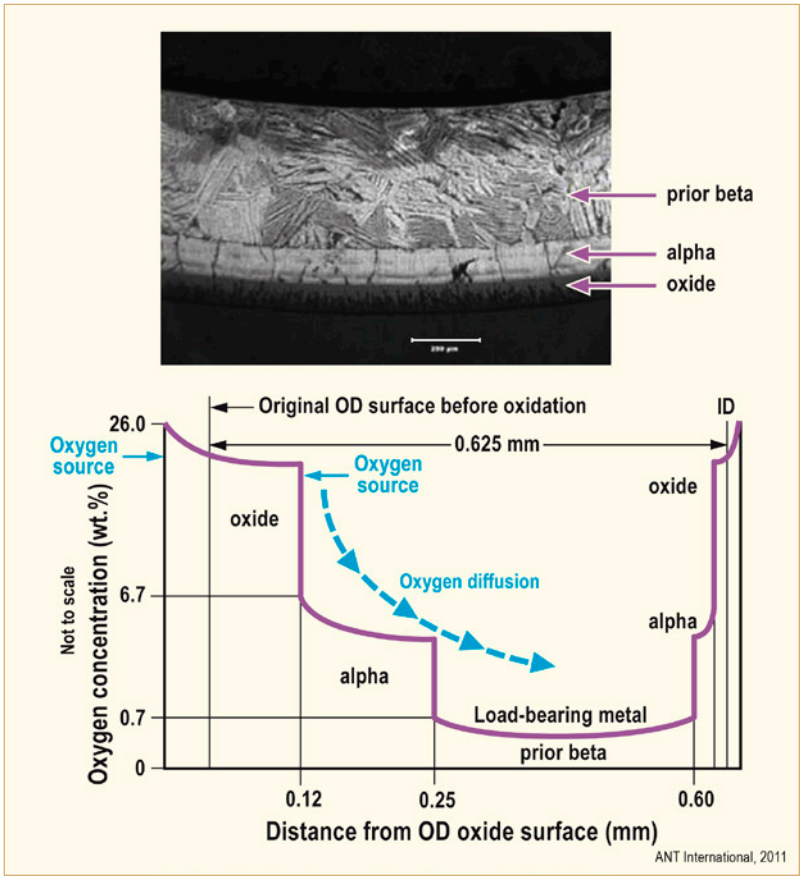

Figure 8-3: Structure of oxidized cladding, after [Meyer, 2013].

- First, the high water and steam temperatures increase their reaction rates with the cladding and increase the conversion of the cladding surface into thicker ZrO_2 films.
- As the LOCA temperature passes the levels where α→β transformations start and finish, the resulting structure consists of:
  - The growing ZrO_2 layer.
  - A brittle zirconium alloy layer with a very high oxygen content which stabilizes the α phase, formed by diffusion of oxygen from the oxide layer.
  - The bulk cladding, which is now in the β phase, has a high solubility for hydrogen; the hydrogen picked up by the cladding from the water-metal reaction increases the solubility of oxygen in the β layer.
- The ZrO_2 and oxygen stabilized α layers grow with continued diffusion of oxygen and hydrogen from the water reaction. The increasing amount of oxygen convert some of the β phase to oxygen stabilized α phase with the concurrent shrinkage of the β phase. The remaining β phase cladding wall thickness is transformed to α phase, or "prior β phase", on cooling and is the only structural part of the cladding that can insure its integrity.

9 Accident tolerant fuel (ATF) – LOCA and Severe Accidents (Peter Rudling)

9.1 Regulation

The NRC position that zirc-UO_2 system LOCA criteria are not appropriate for ATF designs is supported in the letter from NRC to Westinghouse [ML11238A088, 2013]. On the second page of the letter, there is a discussion of using the same LOCA criteria as for zirc- UO_2 systems as a starting point, to prove SiC cladding meets those criteria. The letter explains that, "Demonstrating that ceramic cladding is highly stable in high-temperature steam does not provide an operational limit. To satisfy the requirements of General Design Criterion 35, other criteria must be identified to ensure coolability of the fuel during the design basis LOCA". It would be reasonable to extrapolate these criteria to all non-zirc-UO_2 designs.

Further, in the Federal Register Notice for the 50.46c proposed rule [ML112520249, 2015] it is stated that a number of paragraphs will be added to the regulations "to reserve rulemaking space for future amendments to §50.46c, including any changes that stem from using newly designed fuel and cladding materials". It would be reasonable to extrapolate that reserved placeholders indicate an NRC expectation that new fuel designs will require new rulemaking to establish their ECCS criteria.

9.2 New Results 2013 – 2015

9.2.1 General

The paper by [Kelly & Druenne, 2014], identifies a list of safety-related fuel degradation behaviours, occuring at the 'fuel meat[9]'-cladding-coolant level. Twelve key characteristics are identified in the comparative assessment of safety credentials for new nuclear fuels – *In some cases the information by the authors is incomplete or incorrect and the author of this section of the ZIRAT/IZNA Report have corrected the information which is in italics.*

- Cladding oxidation & hydriding
  - Oxidation and hydriding may affect the fuel metal cladding material. The hydrogen released from the water/cladding reaction and picked up by the cladding may have a significant cladding embrittlement effect at lower temperatures during design basis accident conditions (LOCA, RIA and seismic event) and also during a cask drop accident related to interim dry storage. Developers of fuel with cladding that is not susceptible to such chemical deterioration, can claim a significant safety margin benefit.
- Hydrogen production
  - Safety margin credit can be claimed for fuels using cladding material that is less prone (than Zr) to chemically react to produce H_2. Specifically the exothermic reaction with steam at high temperature is crucial, since this lead to a positive thermal feedback effect during a LOCA.

[9] The term 'fuel meat' is the material that hosts the fissioning component (uranium and/or plutonium) for the fuel. Most commonly this is an oxide ceramic.

- Cladding strain, fatigue & growth
  - New fuels can be credited with safety margin benefits if they use claddings that are less prone to these slow dimensional changes. Such cladding will have higher strain limits, lower growth tendency and better power cycling tolerance. *More important are dimensional changes in the fuel assembly (in PWRs/VVERs) and fuel channels (BWRs) which is not covered in this list. Thus, the new fuel assembly as a whole should be more dimensionally stable.*
- Cladding collapse/lift-off
  - These phenomena relate to the *creep* strength of the cladding material (and to the designed internal pressure for the new fuel). Fuels with claddings with *higher creep strength* can claim to have safety benefits.
- Fission gas release
  - The released fission gas inventory within the fuel rod void (pellet/cladding gap and plenum) is also of interest since it impacts the margins to a) cladding lift-off (se bullet above) and b) creep strain limit during interim dry storage. A lower inventory of fission gases can be considered as a safety-positive feature for a new fuel.
- Pellet-clad mechanical interaction (PCMI)
  - During a reactivity insertion accident (RIA) fuel with higher burnups mail fail due to PCMI *due to the embrittlement effect of hydrides in the fuel cladding*. Resistance to PCMI can be derived from a lower fuel ceramic expansion tendency, *and from a more ductile fuel cladding through lower hydrogen pickup*. Fuels incorporating material with either property can claim safety margin credit against PCMI damage.
- Fuel-clad chemical interaction
  - New fuels having higher resistance to PCI and SCC can be credited with additional safety margin.
- Wear due to abrasion
  - Resistance to fretting *(debris and/or grid to rod fretting)* wear can be claimed as a significant safety benefit for a new fuel-type
- Fuel fragmentation
  - *High burn-up ceramic fuel can fragment into very small fragments that can disperse through the failed cladding into the coolant (which is considered as a non-coolable geometry which is not acceptable by the regulators) during a RIA and/or LOCA. New fuel technologies may offer resistance to tendency to fragmentations*
- Melting
  - Current fuel safety criteria specify that no part of a fuel can melt in the event of a power transient (or during normal operation). New fuel variants with a higher melting point can claim to offer a safety margin benefit.
- *Creep strain*
  - *For Zr alloy cladding, the limiting fuel failure mechanism during interim dry storage is cladding creep and in many countries there is a maximum allowed creep strain of 1 % to ensure that creep rupture does not occur. However, for new cladding materials, the 1% limit may not be applicable, it could be larger or smaller dependant on creep ductility of the material. A fuel technology developer should assess the creep strain limit for the new concept will give adequate margins towards creep rupture. It may also be that other fuel cladding failure mechanisms not operable for Zr alloy claddings may be operable for the new fuel concept.*

- Crud deposition
  - The deposits are usually benign but they impact negatively on the transfer of heat between the fuel and the coolant. A fuel with surfaces that are less prone to crud build-up can claim this property as a safety benefit.

The characteristics described above should be considered in the context of several key fuel safety 'requirements' describing ideal fuel performance in four broad operating scenarios according to the authors:

- A1 – Fuel is to retain its full integrity while operating under normal reactor conditions & during anticipated operational occurrences (AOO).
- A2 – Furthermore, under normal operating conditions & AOOs, changes in the fuel are to be slow, predictable and well within cladding failure margins.
- B – Fuel is to retain its integrity for "as long as reasonably achievable" during the transient accidents involving; loss of coolant (LOCA) or reactivity insertion (RIA). This requirement applies particularly to fuel that has attained high burn-up. Fuel should not fail during less severe power excursions & transients.
- C – In a 'beyond design basis accident' event the fuel must be highly resistant to cladding-breach failure, and also resist fuel dispersal following any such failure.
- D – The fuel is to retain its full integrity while in extended interim dry storage following its discharge from the reactor core. This requirement is of particular significance for fuel that has attained high burn-up.

A short list of promising enhanced-safety fuel types is given in Table 9-1.

Table 9-1: New fuel technology categories, after [Kelly & Druenne, 2014].

Category	Specific enhanced-safety fuel types
'Dispersion' fuels	• UO_2 ceramic containing a high thermal conductivity ceramic (BeO or SiC) additive • Multi-coated fissile particles embedded in a robust matrix of graphite or other thermally conductive material
Thoria-based fuels	• Mixed $(Th,Pu)O_2$ ceramic pellets
Enhanced thermal pathway fuels	• Annular cross-section Zr-clad fuel rods with dual inner & outer surface cooling • All-metal enriched uranium fuel
Robust fuel claddings	• SiC-clad fuels • Stainless steel of molybdenum clad UOX fuel
	ANT International, 2015

From review of reports, papers, and presentations the performance criteria in Table 9-2, Table 9-3 and Table 9-4 were constructed to evaluate potential cladding technologies for further development and testing within the LWR Sustainability (LWRS) Program, [Barrett et al, 2012]

Table 9-2: Identified critical cladding performance parameters which must be met for consideration in further development and testing. See [Barrett et al, 2012] for information about references in the table, after [Barrett et al, 2012].

Critical cladding performance parameters	Zr alloy (standard)	New technology criteria	Comments	Ref#
Maximum operating temp (°C)	650	>650	Temp where structure or oxidation/corrosion becomes limiting	1
Neutron absorption cross section	0.0142 cm^{-1} 0.26 barns	<0.0142 cm^{-1} <0.26 barns	Reduced parasitic absorption	1, 2
U-235 penalty (% increase in U-235 required for equivalent 18 month cycle at constant nominal power)	0	≤0	Equivalent fuel geometry	1
Clad manufacturability (low cost; low complexibilty)	Mfgr 3.05–4.57 ×10^6 m/yr (1); $20-$30 per meter	Mfgr 3.05–4.57 × 10^6 m/yr; (Suggested acceptable increased fabrication costs of up to 50% given power uprates of 10 – 30%) (3)	Must be able to meet current mfg demand – highly complex technologies may be costly and time consuming to manufacture	4
Coolant cladding chemical interaction/degradation	Localized oxidation not to exceed17% of cladding thickness befre oxidation (5)	Not allowed under normal operating conditions of postulated accident conditions		1
Creep (thermal or irradiation)	Creep strain for Zry-4 @ room temp: ~0.66% (7)	≤Zircaloy	Can affect conductivity, fuel clad interactions, and cladding structural integrity	1
Operational lifetime	62 MWd/kg U	>80 MWd/kg U	U-total not U-235. Must be greater than Zr alloy standard	1, 3
Lifecycle net cost of fuel system	8.79 mills/kWeh	<8.79 mills/kWeh	(mill is a unit of measure = 0.001$)	3
High strength/ductility	UTS 437 MPa for Zr4 @ room temp (7)	≥Zr stnd	UTS = Ultimate tensile strength – averaged value between longitudinal and transverse strength	6
Hermeticity			Necessary to contain fission gaes under nominal operating conditions	6
Longer coping times during LOCA	10 hours – dependent on the specific NPP (10 CFR 50.63 & RG 1.155)	>10 hours		8
Hydrogen generation in LOCA (exothermic reaction rate in steam)	Total H production not to exceed 1% of the total amount of H produced if all metal cladding were to react (5)	Minimal H reaction rate		
Power uprates	3411 MWt – typical LWR	10 – 20% increase		3
				ANT International, 2015

10 Dry Storage

All new information related to this topic has been included in Dry Storage Handbook, Fuel Performance in Dry Storage by Patterson C. and Garzarolli F., 2015, [Patterson & Garzarolli, 2015].

The introduction and conclusions in the Handbook is given below (for more information, see the Handbook):

Introduction – A technical assessment of the expected performance of spent nuclear fuel (SNF)[11] during extended dry-storage time periods and the condition of such fuel at the end of dry storage is given in this document. The principal focus of the reviews which follow is on SNF and the effects of dry storage rather than on dry-storage containers and the related storage facilities. The objective is to provide background information on the likely behaviour of materials comprising water reactor fuel assemblies and on the performance of integral assemblies under conditions typical of dry storage for extended intervals of time. In brief, the technical assessment supports a conclusion that, although technical issues have been postulated with regard to long-term storage, there are no high-risk concerns with the extension of dry storage to long times; with proper planning and implementation, the risks are expected to be low.

Dry storage of spent nuclear fuel is a relatively mature technology, which has emerged as the consensus, near-term method in most nuclear countries [Bunn et al, 2001]. As of 2014, spent nuclear fuel elements from commercial power plants and from research reactors have been stored in a dry state for nearly 30 years and 40 years, respectively. This experience involves fuel from a wide range of reactor types; e.g., CANDU, HWR, PWR, BWR, VVER-440, VVER-1000, RBMK, MAGNOX and the HTGR. Storage systems include vaults, concrete canisters, steel-lined concrete containers and metallic casks of various configurations. Although early efforts involved storage-only containers, SNF from commercial power plants is now typically placed in dual-use containers that are intended for both transportation and storage. These dual-use containers are in the form of bolted casks with integral shielding or welded canisters with protective overpacks; i.e., silo (vertical) or bunker (horizontal) structures.

The relative importance of SNF performance during dry storage depends on the expected path of SNF from wet storage through reprocessing or disposal. The goal is for SNF to remain intact at least through post-storage retrieval for reprocessing or placement and sealing in a container at a final disposal repository. There may be cases where safety analyses take credit for SNF integrity beyond dry storage, for example, through some portion of the disposal time period. Such plans could result in the need to analyze performance through thousands to hundreds of thousands of years of disposal. Since the interest here is only for dry storage and some associated handling and transportation, SNF integrity during disposal is not addressed. Since dry storage already has been shown acceptable for tens of years, the emphasis is on any changes that may occur during extensions of the dry-storage time periods to a hundred years, or perhaps several hundred years. Information is included, however, on the expected performance of SNF during both the early and extended stages of dry storage.

In selecting the amount and type of information to present, it is acknowledged that some phenomena are more extensively evaluated and that the available data are more readily available in open sources than for other phenomena. Also, consideration is given to some phenomena being more important, that is, having more risk, than other phenomena. The degrees of coverage reflect these differences.

The information presented is not intended to be the basis for any specific safety or licensing evaluation. Rather, it is intended to improve understanding of issues associated with dry storage.

---

[11] The term “spent nuclear fuel” (SNF) is considered equivalent to “used nuclear fuel” (UNF) in this document.

The importance of SNF integrity during dry storage and associated handling and transportation is influenced strongly by the expected SNF path. There are two fundamental flow paths, each with its advantages and disadvantages.

- Option 1: If SNF is expected to be repackaged after storage, SNF integrity and resilience during handling is very important. An example of this expectation is the planning in Great Britain, where it is assumed that SNF will be repackaged from dry-storage canisters into other containers after a time period on the order of a hundred years. Also, the US Yucca Mountain Repository License Application (YMRLA) was based on the assumption that most SNF would be repackaged into Transportation, Aging, and Disposal (TAD) canister, but that US expectation is no longer certain. Sweden and Finland are selecting a different option; i.e., both plan to package SNF directly into copper canisters for disposal. The repository licenses are still under review, however, so significant delays could result in the need for dry storage, at least in Finland. In most other countries, decisions regarding repackaging have not been finalized.

- Option 2: If SNF is expected to remain in one multipurpose canister (MPC) from initiation of dry storage through disposal of that MPC into a disposal cask, SNF integrity is important but not as important as if repackaging is expected. This SNF path was planned in some early designs of some dry-storage containers and remains an option with significant advantages. This option continues to be considered, for example, by EPRI in Electric Power Research Institute, "Feasibility of Direct Disposal of Dual-Purpose Canisters: Options for Assuring Criticality Control," [EPRI, 2008].

The extent to which each option will be adopted still is to be determined.

Technical issues related to long-term, dry storage of SNF and to subsequent transport and handling have been considered in a number of reviews. For example, the US Nuclear Waste Technical Review Board (NWTRB), in its "Evaluation of the Technical Basis for Extended Dry Storage and Transportation of Used Nuclear Fuel" [NWTRB, 2010], considered and reported on the issues associated with degradation of SNF, metal storage containers, and the concrete overpacks and pads. The NWTRB report acknowledges that there are some technical issues that need better understanding to support extrapolations to long dry-storage times in stating "The review identified references to general metal and concrete deterioration mechanisms and modelling, but none included the information necessary to predict the degradation of dry-storage canisters, casks, or concrete structures during extended storage." In the context of the complete NWTRB report, this statement is interpreted as indicating that dry storage to hundreds of years is supportable technically but that it would be beneficial for some technical concerns to have more data or better understanding. Related studies by the US Department of Energy [DOE, 2012], Nuclear Regulatory Commission [NRC, 2012], International Atomic Energy Agency and an Extended Storage Collaboration Program (ESCP) [EPRI, 2011] identified and prioritized technical gaps. These gaps and their relative importance vary among countries and organizations, but are similar in many respects. The review given in [DOE, 2012] and summarized in Table 10-1 considered gaps and priorities of the programs and countries in that participated in the reviews noted above. Issues are listed in Table 10-1 according to the approximate priorities as perceived by the DOE.

11 Trends and needs

Improved fuel reliability and operating economics are the driving forces for changing operating conditions, while at the same time maintaining acceptable margins to operating and regulatory safety limits. Table 11-1 gives the trends for BU achieved compared to regulatory limits in various countries. An approximate ("rule of thumb") conversion of BU to fluence is 50 GWd/MT is equivalent to about 1×10^{22} n/cm^2, E>1 MeV (or about 17 dpa), but this depends on many nuclear parameters such as enrichment, extent of moderation and neutron energy spectrum. In general PWRs operate to higher discharge BUs compared to BWR because of higher PWR power densities and neutron fluxes, but the differences are decreasing with time. There are some incentives to reach BUs of 60-70 GWd/MT batch average, but the economic values of doing so are decreasing. A majority of US plants and many in Europe have undergone power uprates, from a few percent to up to 20%. This increases the number of FAs in a core that operates at high power, thereby decreasing the margin to established limits. In cooperation with utilities, fuel suppliers have operated LTA or LUAs to very HB, in some cases approaching 100 GWd/MT peak rod exposures.

Table 11-1: Maximum BUs achieved vs. regulatory limits, (excludes LTAs).

	BU (GWD/MT)				
Country	**Batch**	**Assembly**	**Rod**	**Pellet**	**Regulatory Limit**
USA	57	58	62	73	62.5 peak rod
Belgium		50-55			55 UO_2 assy., 50 MOX assy.
Czech Republic	51	56	61		60 peak rod
Finland	45.6*	48.6	58		57 assy. (for PWR)
France	47	51 UO_2 42 MOX			52 assy.
Germany	58	62	68		65 assy.
Hungary		50	62		
Japan	50	55	62		55 UO_2 assy., 45 MOX assy.
Korean Republic	46				60 rod
Netherlands	52	55	59		60 rod
Russia	60	65			
Spain	50.4	57.4	61.7	69	
Sweden	47	57.2	63.6	65	60 assy., 64 rod
Switzerland	64	68	73		80 pellet
Taiwan					60 rod (P), 54 assy. (B)
UK	44.3	46.5	50		55 pellet
Ukraine		50			
*Current batch design for 50 GWD/MT in BWR					
ANT International, 2014					

As discussed in earlier sections as BU and fluence become higher, material properties and microstructure evolve. Examples include:

- In PWRs it is found the Zry-4 no longer meets corrosion and hydriding needs; therefore virtually all current PWR cladding use a zirconium alloy containing Nb.
- Although not a new phenomena, observed SPP dissolution and re-precipitation phenomena have required a new perspective on alloy development and HPU.
- BWR channel bow at HB has required a new understanding of the relationships between HPU, shadow corrosion and irradiation growth.

A broader listing of issues needing resolution include:

- Corrosion related to oxide thickness and H pickup:
  - BWRs and PWRs:
    - Mechanism of solid hydrides on corrosion mechanism.
    - Effect of Nb.
  - BWRs:
    - Shadow corrosion mechanisms and its relation to channel bow.
    - Late increased corrosion and HPU of Zry-2 at HBs.
    - Localised hydriding – Browns Ferry – new failure mechanism
    - CRUD-chemistry-corrosion interaction.
    - Effect of water chemistry impurities, as well as specific effects of NMCA, with or without Zn-injection.
  - PWRs:
    - Effects of surface contaminations and/or boiling on Zr-Nb alloys.
    - Welding of the new alloys may need improved processes (Zr-Nb alloys).
    - Effect of increased Li together with increased duty (sub-cooled boiling) with and without Zn-injection.
    - Effects of increased hydrogen coolant content (to mitigate Primary Water Stress Corrosion Cracking (PWSCC)).
    - Axial offset anomaly (AOA) mechanisms.
- Mechanical properties related to irradiation and H pickup:
  - Decreased ductility and fracture toughness as consequence of the increased HPU and formation of radial hydrides during any situation (e.g., RIA, PCMI, LOCA and post-LOCA events, seismic event, transport container drop-accident conditions).
  - Quantification of the effect of irradiation on solubility of hydrogen, and mechanism by which the phenomenon occurs.
  - Details of deformation mechanisms in zirconium alloys, including being able to predict the dislocation channelling system.
  - Development of micromechanical models applicable to deformation at appropriate component conditions.
  - DHC mechanism (degradation of failed fuel, outside-in cracking and dry storage).

12 References

10 CFR Part 100.11, *Determination of Exclusion Area, Low Population Zone, and Population Centre Distance*, U.S. Government Printing Office, Washington, 1990a.

10 CFR Part 50 Appendix A, *General Design Criteria for Nuclear Power Plant*s, U.S., Government Printing Office, Washington, 1990b.

Adamson R. B. and Bell W.L., *Effects of Neutron Irradiation and Oxygen Content on the Microstructure and Mechanical Properties of Zircaloy*, Microstructure and Mechanical Behaviour of Materials, Proceedings: Int'l Symposiums, Xian, China, Oct. 1985, EMAS, Warley, UK, 237-246, 1986.

Adamson R. B., *Recovery of Irradiation Damage by Posts-Irradiation Thermal Annealing-Relevance to Hydrogen Solubility and Dry Storage Issues*, EPRI Technical Report 1013446, June 2006.

Adamson R. B., Cox B., Garzarolli F., Sabol G. Strasser A. and Rudling P., *ZIRAT12/IZNA7 Annual Report*, ANT International, Mölnlycke, Sweden, 2007a.

Adamson R., Garzarolli F., Cox B., Strasser A. and Rudling P., *Corrosion Mechanisms in Zirconium Alloys*, ZIRAT12/IZNA7 Special Topics Report, ANT International, Mölnlycke, Sweden, 2007b.

Adamson R. B., Garzarolli F. and Patterson C., *In-Reactor Creep of Zirconium Alloys*, ZIRAT14/IZNA9 Special Topic Report, ANT International, Mölnlycke, Sweden, 2009a.

Adamson R. B., Garzarolli F., Patterson C., Rudling P. and Strasser A., *ZIRAT14/IZNA9 Annual Report*, ANT International, Mölnlycke, Sweden, 2009b.

Adamson R. B., Garzarolli F., Patterson C., Rudling P. Strasser A. and Coleman K., *ZIRAT15/IZNA10 Annual Report*, ANT International, Mölnlycke, Sweden, 2010.

Adamson R. B., Garzarolli F., Patterson C., Rudling P., Strasser A., Coleman K. E. and Lemaignan C., *ZIRAT16/IZNA11 Annual Report*, ANT International, Mölnlycke, Sweden, 2011.

Adamson R. B., *Charged Particle Bombardment in Zirconium Alloys – A Review*, ZIRAT19/IZNA14 Special Topic Report, 2014.

Amaya M., Nagase F., Sugiyama T., Udagawa Y., Narukawa T. and Sawada A., *Current Studies at JAEA on Fuel Behaviors under Accident Conditions*, Proceedings of WRFPM 2014, Paper No. 100086 Sendai, Japan, Sep. 14-17, 2014.

Amaya M., Udagawa Y., Narukawa T., Mihara T. and Sugiyama T., *Behavior of High Burnup Advanced Fuels for LWR During Design-Basis Accidents*, Top Fuel 2015.

Ammon K., Loner H., Bieli R. and Ledergerber G., *Monitoring the Integrity of Control Rods On-Line with a Helium Leak Detector*, TopFuel 2015, Zürich, Switzerland, 2015.

Andersson B., Bergmann U., Dahlbäck M., Hallstadius L., Haskins W. and Limbäck M., *Advantages Gained by Introducing Low Tin ZIRLO as BWR Channel Material*, TopFuel 2015, Zürich, Switzerland, 2015a.

Andersson B., Tonks M., Casillas L., Vyas S., Nerikar P., Uberuaga B. and Stanek C., *Multiscale Simulation of Xenon Diffusion and Grain Boundary Segregation in UO_2*, Journal of Nuclear Materials, Vol. 462, pp. 15-25, 2015b.

Andresen P. and Carter R., *Development and Analysis of an Alloy X-750 SCC Growth Rate Database*, 17th International Conference on Environmental Degradation of Materials, Ottawa, Ontario, Canada, August, 2015.

Anonymous, *Standard test methods for elevated temperature tension tests of metallic materials*, ASTM International, E21-09 (Approved 2009).

Anonymous, *Standard Specification for Wrought Zirconium and Zirconium Alloy Seamless and Welded Tubes for Nuclear Service (Except Nuclear Fuel Cladding)*, ASTM International, B353-07 (Revised 2012).

Anonymous, *Standard Specification for Wrought Zirconium Alloy Seamless Tubes for Nuclear Reactor Fuel Cladding*, ASTM International, B811-07 (Approved 2013a).

Anonymous, *Canadian Standards Association, Technical Requirements for In-service Evaluation of Zirconium Alloy Pressure Tubes in CANDU Reactors*, Update 2, N285.8-10, 2013b.

Anonymous, *Standard Test Method for Determining Threshold Stress Intensity Factor for Environment-Assisted Cracking of Metallic Materials*, ASTM International, E1681, (Approved 2013c).

Anonymous, *Standard test methods for tension testing of metallic materials*, ASTM International, E8/E8M-15 (Approved 2015).

Arkoma A., Hänninen M., Rantamäki K., Kurki J. and Hämäläinen A., *Statistical analysis of fuel failures in large break loss-of-coolant accident (LBLOCA) in EPR type nuclear power plant*, Nuclear Engineering and Design 285, 1–14, 2015.

Bair J., Zaeem M. A. and Tonks M., *A review on hydride precipitation in zirconium alloys*, J. Nucl. Mater., 466, pp.12-20, 2015.

Bales M., *Personal Communication*, 2015.

Barrett K., Bragg-Sitton S. and Galicki D., *Advanced LWR Nuclear Fuel Cladding System Development Trade-off Study,* INL Report INL/EXT-12-27090, 2012.

Bauer K. et al., *Electrochemical examinations in 350°C water with respect to the mechanism of corrosion-hydrogen pickup*, ASTM STP 1354, pp. 836-852, 2000.

Besmann T. M., Ferber M. K., Lin H-T. and Collin B. P., *Fission product release and survivability of UN-kernel LWR TRISO fuel*, Journal of Nuclear Materials 448, pp. 412–419, 2014.

Bianco A., Vitanza C., Seidl M., Wensauer A., Faber W. and Macian-Juan R., *Experimental investigation on the causes for pellet fragmentation under LOCA conditions*, Journal of Nuclear Materials 465, 260-267, 2015.

Blackmur M. S. et al., *Zirconium hydride precipitation kinetics in Zircaloy-4 observed with synchrotron X-ray diffraction*, J. Nucl. Mater., 464, pp.160-169, 2015.

Blair P., Khvostov G., Romano A., Hellwig C. and Chawla R., *Nuclear Science and Technology*, Vol. 45, pp. 639-646, 2008.

Blake E. M., *US Capacity factors: Keeping the grid stable*, Nuclear News, May, 2015.

Bosch R., Vankeerberghen M., Gérard R. and Somville F., *Crack Initiation Testing of Thimble Tube Material under PWR Conditions to Determine a Stress Threshold for IASCC*, Journal of Nuclear Materials, Vol. 461, pp. 112-121, 2015.